NASA CR-54667

DIAGNOSTICS OF MHD GENERATOR PLASMAS

by

C. H. Kruger, M. Mitchner, and R. H. Eustis

prepared for

NATIONAL AERONAUTICS AND SPACE ADMINISTRATION

CONTRACT NAS 3-6261

PLASMA GASDYNAMICS LABORATORY
MECHANICAL ENGINEERING DEPARTMENT
STANFORD UNIVERSITY ■ STANFORD, CALIFORNIA

DIE LUFT DER FREIHEIT WEHT

Requests for copies of this report should be referred to

National Aeronautics and Space Administration
Office of Scientific and Technical Information
Attention: AFSS-A
Washington, D.C. 20546

132

NASA CR-54667

SUMMARY REPORT

DIAGNOSTICS OF MHD GENERATOR PLASMAS

by

C. H. Kruger, M. Mitchner, and R. H. Eustis

prepared for

National Aeronautics and Space Administration

February 28, 1967

CONTRACT NAS 3-6261

Technical Management
NASA Lewis Research Center
Cleveland, Ohio
Spacecraft Technology Division
N. John Stevens

Plasma Gasdynamics Laboratory
Department of Mechanical Engineering
Stanford University, Stanford, California
94305

ABSTRACT

A noble-gas MHD generator was constructed and its performance measured. Wall leakage and Hall effects seriously degraded the generator performance. A spectroscopic "interference-filter photographic" technique was devised for spatially resolving the electron temperature distribution, and microwave measurements showed non-equilibrium electron concentration after expansion in a supersonic nozzle. The effect of the electric field on the electron distribution function was determined, and procedures for calculating electrical conductivity and Hall parameter were evaluated. Theoretical calculation of current distribution in segmented MHD generators showed important effects of temperature or conductivity gradients.

Table of Contents

DIAGNOSTICS OF MHD GENERATOR PLASMAS

by

C. H. Kruger, M. Mitchner, and R. H. Eustis
Plasma Gasdynamics Laboratory, Stanford University

1.0 SUMMARY

A research program was conducted between 28 September 1964 and 27 September 1966 to investigate plasma diagnostics in connection with noble-gas MHD generators. A major motivation for this work was the failure of noble-gas MHD generators to operate as expected from available theories. One reason for the poor experimental performance was believed associated with current concentrations on electrodes due to the Hall effect. It was hoped that this program would develop diagnostic techniques which would afford a better knowledge of the current distribution under MHD generator operating conditions.

A spectroscopic "interference-filter photographic" technique was developed for spatially resolved electron-temperature measurements in a gas discharge. Measurements were made with an electric field applied to a single pair of electrodes in a flowing, atmospheric-pressure, partially ionized plasma. The plasma was produced by the arc-jet facility with the use of potassium sodium seeding. Plasma temperatures were approximately 2000°K and electrode temperatures approximately 900°K. Electron-temperature distributions were obtained for a variety of prebreakdown and postbreakdown (arc) conditions. The measurements were supported by analytical studies of the population temperature of sodium resonance lines and of the effects on the relative-intensity measurements of self-absorption resulting from low-temperature boundary layers.

The electron number density entering an MHD generator test section downstream of a nozzle may in principle be out of equilibrium with both the electron and the heavy-particle temperatures. Experiments using microwaves were performed to measure the electron number density upstream and downstream of a supersonic expansion of seeded argon. At a stagnation temperature of 1950°C and at a seeding fraction of 0.1%, it was determined that the electron number density was in fact considerably out of equilibrium with the gas temperature. The experimental results were in close agreement with theoretical calculation, and show that the electron number density tends to freeze at Mach numbers in excess of about 0.4.

An open-system arc-heated argon and helium apparatus was constructed which permitted gas temperatures up to 2000°K at both subsonic and supersonic velocities in the 2 cm x 5 cm x 30 cm-long test section. Open-circuit voltage and short-circuit currents as high as 13 volts and 0.04 amperes per electrode pair were measured, although internal shorting through conducting layers on the wall precluded definitive experiments.

The effects of wall leakage and conductivity nonuniformities on MHD generator performance were calculated analytically. It was shown that these effects could very seriously degrade performance, particularly for high values of the Hall parameter.

The properties of a two-temperature, partially ionized plasma have been analyzed theoretically by means of a spherical-harmonic expansion of the electron Boltzmann equation. In the case where nonelastic collisions are neglected, the transition of the distribution function from the weak-ionization form to an elevated-temperature Maxwellian has been demonstrated numerically. Various plasma regimes have been delineated. Under the experimental conditions of Kerrebrock and Hoffman* and Cool and Zukoski**, no significant departures from a Maxwellian distribution are predicted by these numerical solutions. In addition, the rate equations for the electron density, coupled with the solution of the Boltzmann equation, have been used to study deviations from the Saha equation. Preliminary results showing large deviations for some cases have been obtained to date.

When a partially ionized gas is subjected to applied electric and magnetic fields, $\underline{E}$ and $\underline{B}$ respectively, the resulting current density is $\vec{J} = \sigma^{\parallel}\underline{E}^{\parallel} \mp \sigma^{\perp}\underline{E}^{\perp} + \sigma^{H}\,\hat{B}\times\underline{E}$, where $\underline{B} = B\hat{B}$, $E^{\parallel} = \underline{E}\cdot\hat{\underline{B}}$, and $\underline{E}^{\perp} = \underline{E} - \underline{E}^{\parallel}$. Using the fact that the electron mass is much less than the mass of any other particle, it has been shown first that the conventional Chapman-Enskog calculation of the tensor conductivity ($\sigma^{\parallel}$, $\sigma^{\perp}$, σ^{H}) may be considerably simplified so as to require the inversion of matrices whose order depends only on the degree of the approximation, but whose order is independent of the number of species. Secondly, a mixture rule has been proposed for the calculation of $\sigma^{\perp}$ and σ^{H}, which simplifies the necessary computation even more. (The Hall parameter is then also obtained as the ratio $\beta \equiv \sigma^{H}/\sigma^{\perp}$.) For a wide range of speed-dependent collision cross sections and Hall parameters, and for all degrees of ionization, it has been shown that the proposed mixture rule yields results which are within a factor of about 15% of the more accurate Chapman-Enskog results.

---

*AIAA J. 2, 1080 (1964).

**Sixth Symposium on Engineering Aspects of MHD (1965).

Calculations of the performance of an MHD generator with segmented electrodes have previously been performed under the assumption of a uniform electrical conductivity. These calculations have shown that the presence of a transverse magnetic field leads to a severe concentration of current at one edge of each electrode. If this situation were in fact to occur, it would lead to a severe nonuniformity in the electrical conductivity and thereby would lead to the question of the significance of constant conductivity calculations. In the present study, calculations were therefore performed on the effect of nonuniform electrical conductivity on segmented-generator performance. Two kinds of calculations were performed. In the first, conductivity profiles were specified; in the second, a self-consistent calculation was performed in which the electrical conductivity was determined through the electron energy equation and the Saha equation at the electron temperature. The results of both kinds of calculations showed that nonuniformities lead to a deterioration in generator performance. With a low conductivity layer of gas adjacent to the electrode surface, the concentration of current density distribution is reduced, and this result is consistent with experimental evidence. For the second type of calculation, it was shown that the governing equations change from being elliptic to being hyperbolic when the Hall parameter exceeds a value of about one. The condition for this change in character of the equations was shown to correspond to the occurrence of a physical instability, in which the rate of Joule heating of the electrons exceeds the rate at which the electrons can transfer energy to the heavy particles.

2.0 INTRODUCTION

The generation of magnetohydrodynamic power by utilizing a seeded noble gas has met with remarkable difficulties considering the simplicity of the concept. In 1961, Kerrebrock [1] described a phenomenon which would permit electron temperatures greater than heavy particle temperatures in the presence of an electric field, provided that electron-heavy particle collisions were energetically inefficient even for atmospheric pressure plasmas. This concept as shown by Sutton [2] holds promise of lower gas temperatures for satisfactory electrical conductivities and power densities. Consequently, many blow-down and loop experiments [3,4,5,6] were initiated, and none has shown performance approaching that predicted by the 1961 theory. Reasons have been suggested for this disappointing performance and electrode current concentrations related to the Hall parameter with associated internal shorting [7] have been seriously considered.

The research program described in this report, which was initiated on 28 September 1964 for a period of two years, was undertaken to make diagnostic investigations in flowing plasmas similar to those used in noble-gas MHD generators. In particular it was desired to spatially resolve plasma properties such as electron temperature and density. Also, it was desired to construct a seeded, noble-gas MHD generator and to measure electric fields and current distributions under operating conditions. Good success was achieved in spatially resolved electron temperature measurements and in calculation of current distribution and plasma properties. In common with efforts at other laboratories, successful operation of a noble-gas MHD generator was not achieved in the contract period, although open-circuit voltages as high as 12 volts and short-circuit currents as high as 0.04 amperes per electrode pair were recorded. Considerable technical difficulty was encountered with conducting layers formed by reaction of a gas impurity (tungsten from the plasma source) and the MHD channel wall material.

The body of this report describes both the experimental and theoretical work conducted during the research program and is reported in detail in Quarterly Progress Reports [8-14]. Most of this work was carried out by graduate students who made very significant contributions to the program. These students were G. F. Hohnstreiter, J. L. Kurz, F. H. Morse, D. A. Oliver, S. Schweitzer, J. F. Shaw, and J. R. Viegas. In addition, staff members of the Plasma Gasdynamics Laboratory, Dr. W. V. Simpkinson, Mr. John R. McLean, Mr. John C. Cutting, and Mr. Frank Levy, were essential to the progress made. Finally, the assistance of Mr. N. John Stevens, NASA Technical Manager, is gladly acknowledged.

3.0 EXPERIMENTAL PROGRAM

3.1 Spectroscopic Measurements

With the objective of the spatially resolved measurement of electron temperature and electron density, a variety of spectroscopic techniques were investigated. A general discussion of such measurements and a detailed list of references are given by Griem [15]. The Jarrell-Ash scanning monochromator was used with the small seeded flame of the Perkin-Elmer burner and with the argon plasma facility to assess the utility of the various methods under the plasma conditions of interest. Initial electron-temperature measurements employed sodium-line reversal [11]. Although this method was satisfactory applied to local measurements, it was found that spatial resolution of electron temperature was more readily obtained by means of the Interference-Filter Photographic technique which is discussed below.

With respect to electron-density measurements, a rotating quartz refractor plate assembly was designed and built [12] for use with measurements of Stark broadening and shifting. It was found, however, that under the pertinent plasma conditions profile measurements on the weak lines for which the Stark effect is the dominant broadening mechanism were not successful. The problem was due to excessive dark current noise in the photomultiplier. Cooling the photomultiplier to -100°C and limiting the bandwidth improved the situation, but not enough to make meaningful profile measurements. Nonetheless, the refractor plate assembly has proved a useful tool in the other spectroscopic measurements. As an alternate approach to the electron-density problem, absolute line-intensity measurements were investigated [13]. This method relies on the tendency of the higher-lying states in the alkali-metal atoms in question to be in local collisional equilibrium with free electrons, whether or not the free electrons are in local equilibrium with the ground state. The intensities of fifteen multiplets from the spectra of sodium and potassium were measured in the flame produced by the Perkin-Elmer burner, and a successful absolute-intensity measurement of the Na 8183-8194 lines was made in a full-scale argon-plasma experiment [14]. Although the method appears feasible, it was not possible in the time available to apply it to the intended applications.

The most useful spectroscopic technique investigated was the Interference-Filter Photographic (IFP) method [12]. By means of the IFP method, spatially resolved electron-temperature measurements are possible over the entire plasma area available for observation at a given instant of time. In this method a narrow-band-pass interference filter is mounted in the optical system between the plasma source and a spectroscopic plate to be exposed by means of a 4" x 5" camera. The interference filter passes only the radiation emitted by the spectral lines under consideration and thus serves the same purpose as the spectrometer. When a photograph is taken of the plasma through the appropriate lens system, the resulting image on the spectroscopic plate is a record of the point-to-point emission of the plasma. From microdensitometer transmission measurements taken over the developed spectroscopic plate, relative temperature measurements can be deduced using the equations developed in Reference 11.* Calibration of the individual spectroscopic plates is obtained by means of a specially constructed step filter of vacuum-deposited chromium on glass and by use on the various plates of a calibration mark from a standard intensity source. The IFP method results in a "temperature photograph" of the plasma, combining photographic flow visualization with relative temperature measurements. Such electron-temperature distributions can be used in conjunction with voltage-probe measurements and the electron-energy equation to infer current-density distributions.

*The data-reduction techniques in current use are similar but somewhat more refined than those discussed in Reference 11.

Laboratory experiments with the Perkin-Elmer burner and a water-cooled stainless-steel tube have shown that exposure times for 103F spectroscopic plates are of the order of 1/10 to 1/50 second, thus permitting some time resolution of the temperature field. The correlation between measured temperature values by means of the IFP method and reversal-temperature measurements was very good, and temperature profiles observed compared very favorably to values obtained by the spectrometer-photographic method taken at the same time [12].

The applicability of the IFP method was supported by two theoretical studies. The relationship of the population temperature for the upper state of the Na 5890 resonance lines, used for the most extensive IFP measurements, to the electron temperature was investigated by means of the collisional and radiative rate equations for that state [12]. It was found that for the small values of the resonance-radiation escape parameter for conditions of interest, the departure of the Na 5890 population temperature T_p from the electron temperature is small*, whether or not the plasma is otherwise in local equilibrium. In the second study, the influence of temperature boundary layers on relative line intensities, and hence the IFP method, was assessed by means of a numerical solution of the equation of radiative transfer for the Na 5890 resonance lines. Various nonisothermal temperature distributions and nonuniformities in seed density corresponding to possible experimental conditions were considered. The intensity of radiation emitted from the plasma was calculated as a function of wavelength throughout the profile of the lines. Although, as expected, the absolute intensity emitted was found to depend strongly on the nonuniformities, calculated relative integrated intensities for reasonable conditions were in remarkable agreement with the relative values of total emission under conditions in the core of the plasma. Thus these results indicate that the relative measurements inherent in the IFP method are insensitive to such boundary-layer variations.

IFP measurements of spatially resolved electron temperature were made under a variety of experimental conditions, first with the Perkin-Elmer burner and then in connection with full-scale argon-plasma experiments. Both the Na 5890 resonance lines and the transparent Na 8183 lines were used. In addition to the agreement noted previously between relative-temperature measurements using IFP and reversal methods, temperature distributions under zero-current conditions in the argon facility obtained by the IFP method were found to correspond closely to distributions measured by means of high-temperature thermocouples.

Typical results from the IFP measurements are shown in Figures 1 through 6. These measurements were made in connection with a gas-discharge experiment using an externally

*Revised values of the radiation-escape parameter, calculated by the method of Holstein [16], were found to be substantially greater than those of Reference 12. The results presented herein are corrected accordingly for the relatively small difference between T_p and T_e.

applied electric field and a 0.1 per cent potassium-seeded argon plasma at one atmosphere pressure, a gas temperature of approximately 2000°K, and electrode temperatures of approximately 900°K. Figures 1 and 2 show a photographic reproduction of the IFP spectroscopic plate and temperature contours obtained therefrom, under conditions of zero applied field. Figures 3 and 4 were obtained under prebreakdown conditions of 80 volts and .060 amps. Figures 5 and 6 show the discharge and temperature contours after breakdown at 104 volts and 4.90 amps.

3.2 Microwave Measurements of Electron Density in an Expanding Flow

The purpose of this investigation was to determine experimentally the axial profile of the electron number density in a weakly ionized, seeded argon gas expanding through a nozzle. The following assumptions were made in the theoretical analysis:

(1) The flow of the argon gas is steady, adiabatic, inviscid, and one-dimensional.
(2) Recombination occurs in the gas phase only; surface recombination and electron attachment are neglected.
(3) The expansion begins from an equilibrium condition in the stagnation region.

In addition, it was assumed that the ionization and recombination reactions of the seed are uncoupled from the flow. This assumption is justified for weakly ionized gases. In this case a one-dimensional isentropic solution for the expansion of the argon through the nozzle provides the temperature and pressure profiles. As the gas flows downstream the temperature and pressure fall and the balance between ionization and recombination shifts in favor of recombination. If the recombination reaction rate is sufficiently fast, the electron number density will be approximately that given by the equilibrium Saha equation at this local temperature and pressure. If the recombination reaction rate is relatively slow, the electron-number-density profile tends to level off, or freeze, resulting in a profile between that corresponding to the stagnation temperature and that corresponding to the considerably lower equilibrium profile.

This nonequilibrium profile may be obtained by solving the electron conservation equation with an appropriate ionization-recombination rate equation. It was assumed that the dominant reactions are electron-atom ionization and three-body recombination

$$e + K \leftrightarrows e + e + K^{+}$$

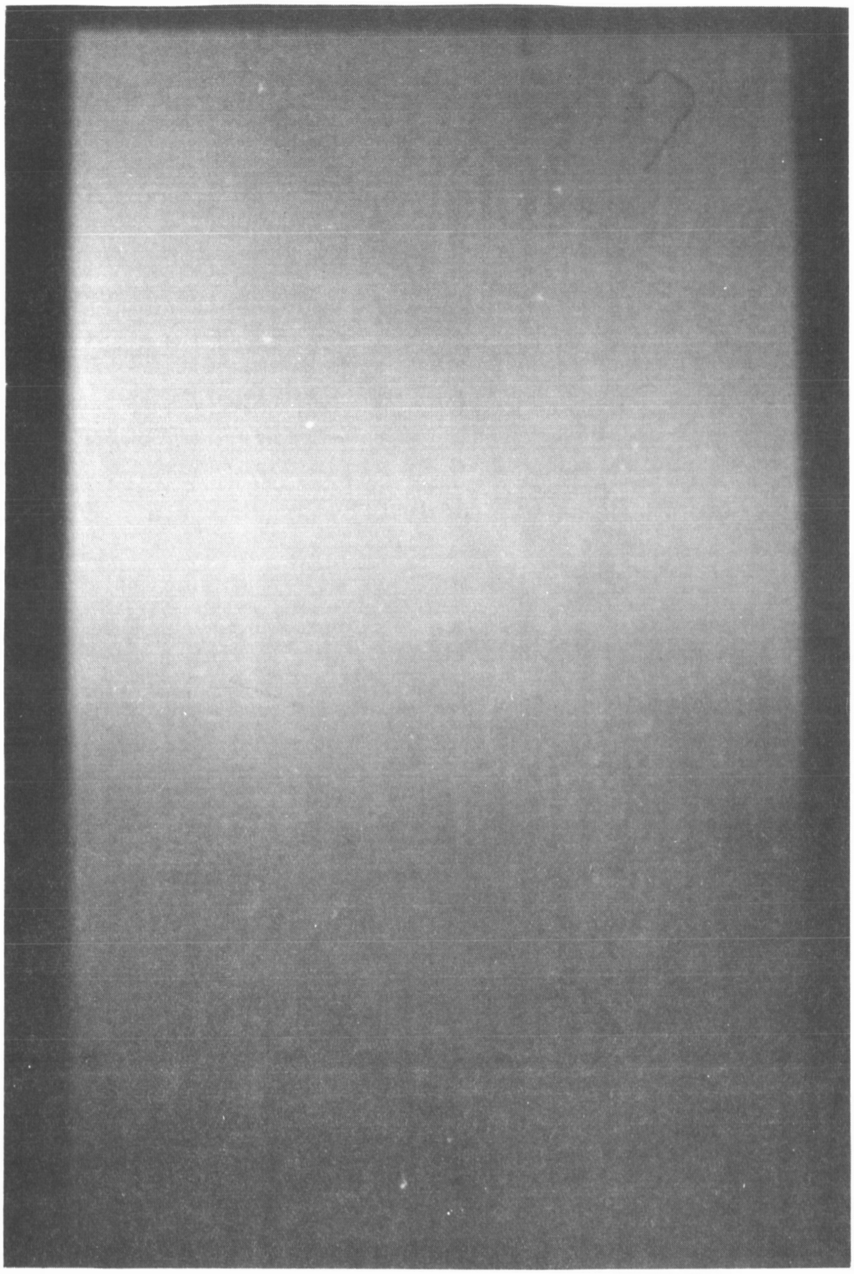

Figure 1. IFP photograph at zero current.

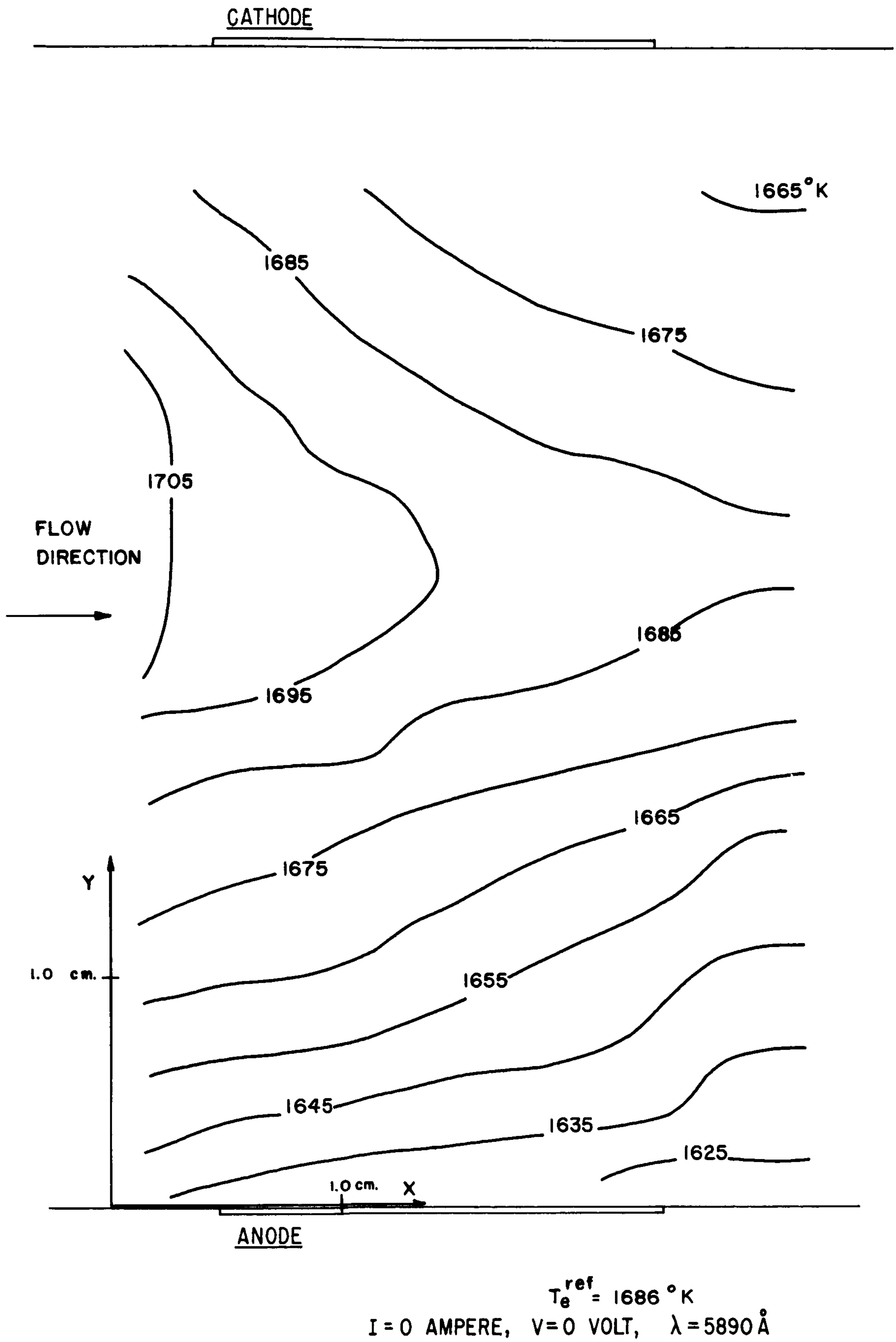

Figure 2. Temperature contours at zero current.

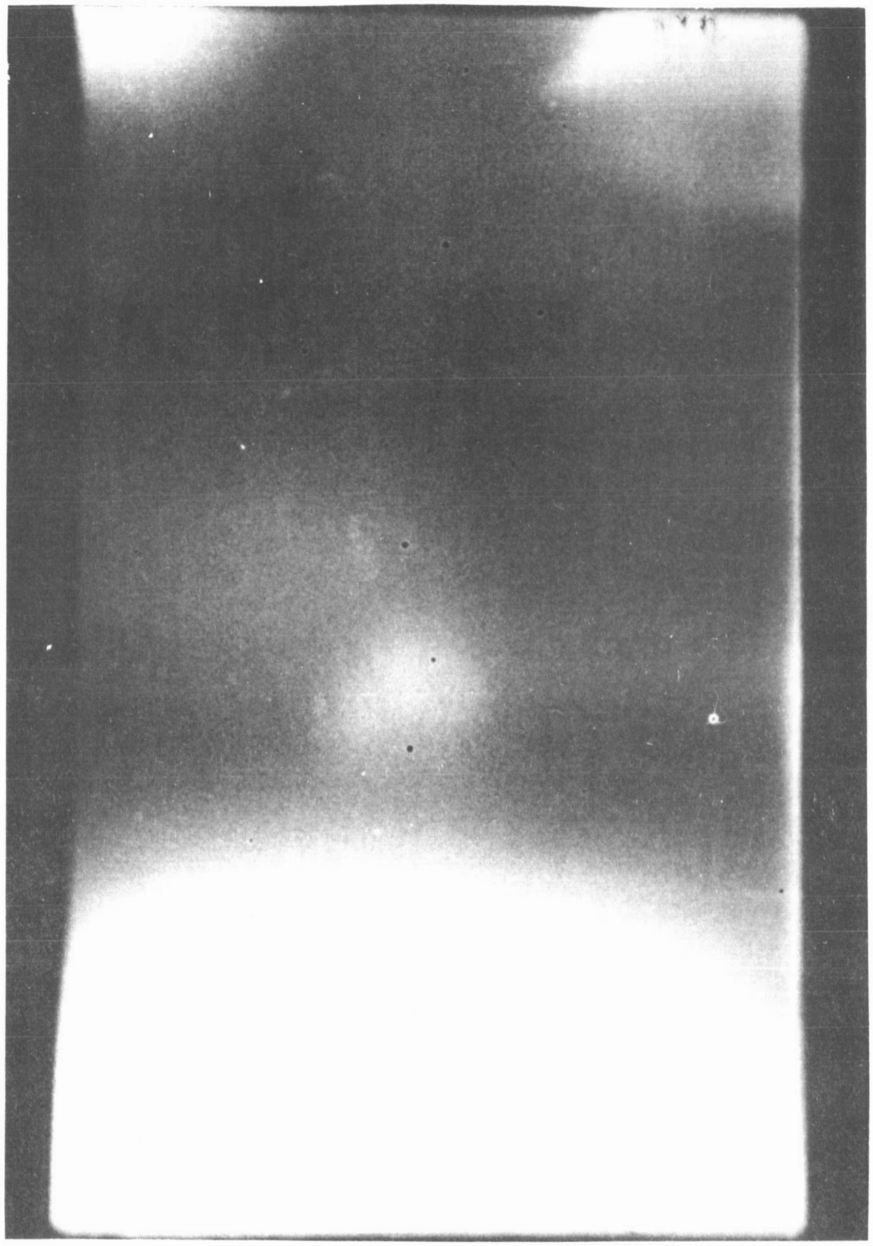

Figure 3. IFP photograph, prebreakdown discharge.

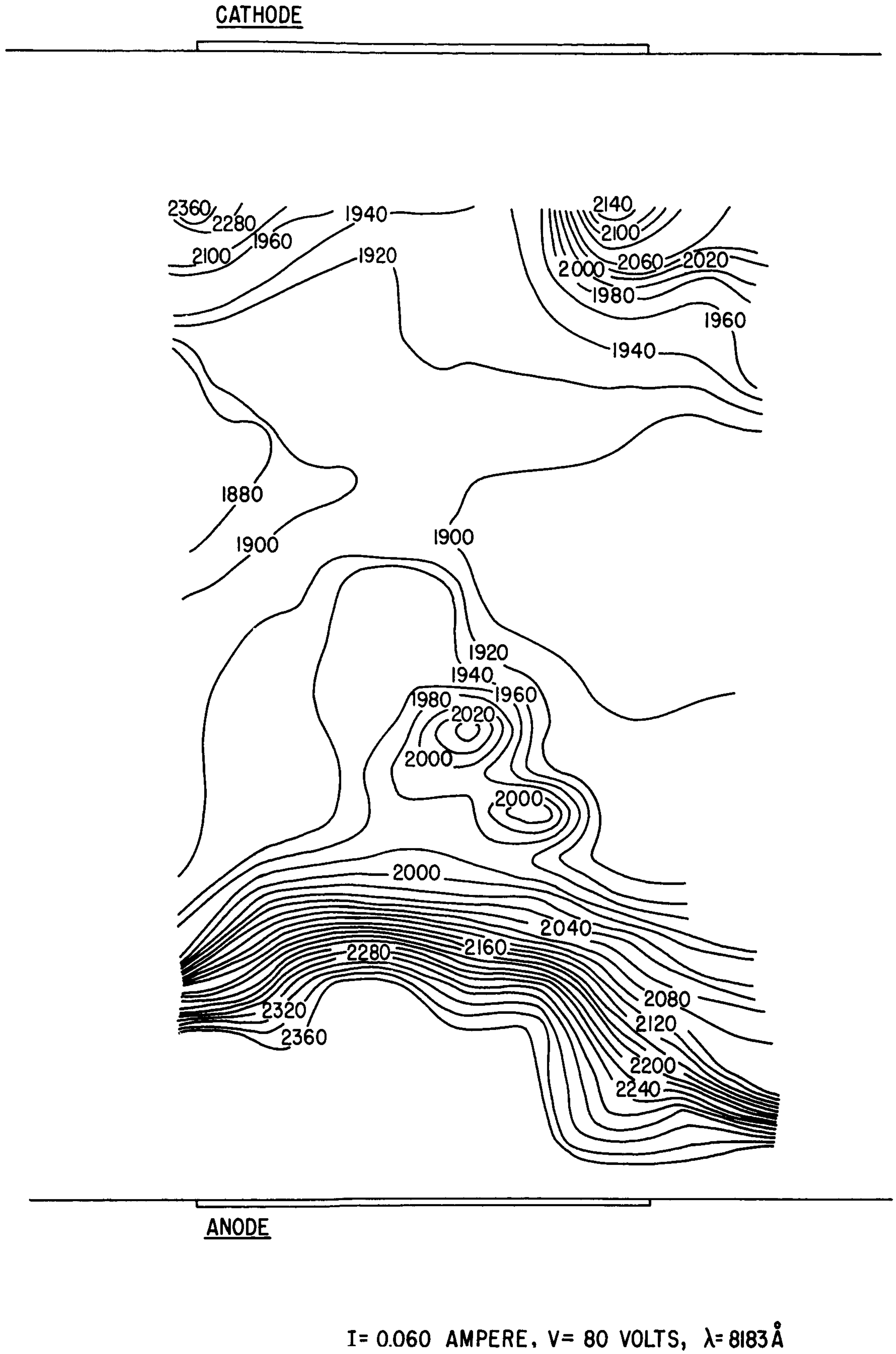

Figure 4. Temperature contours, prebreakdown discharge.

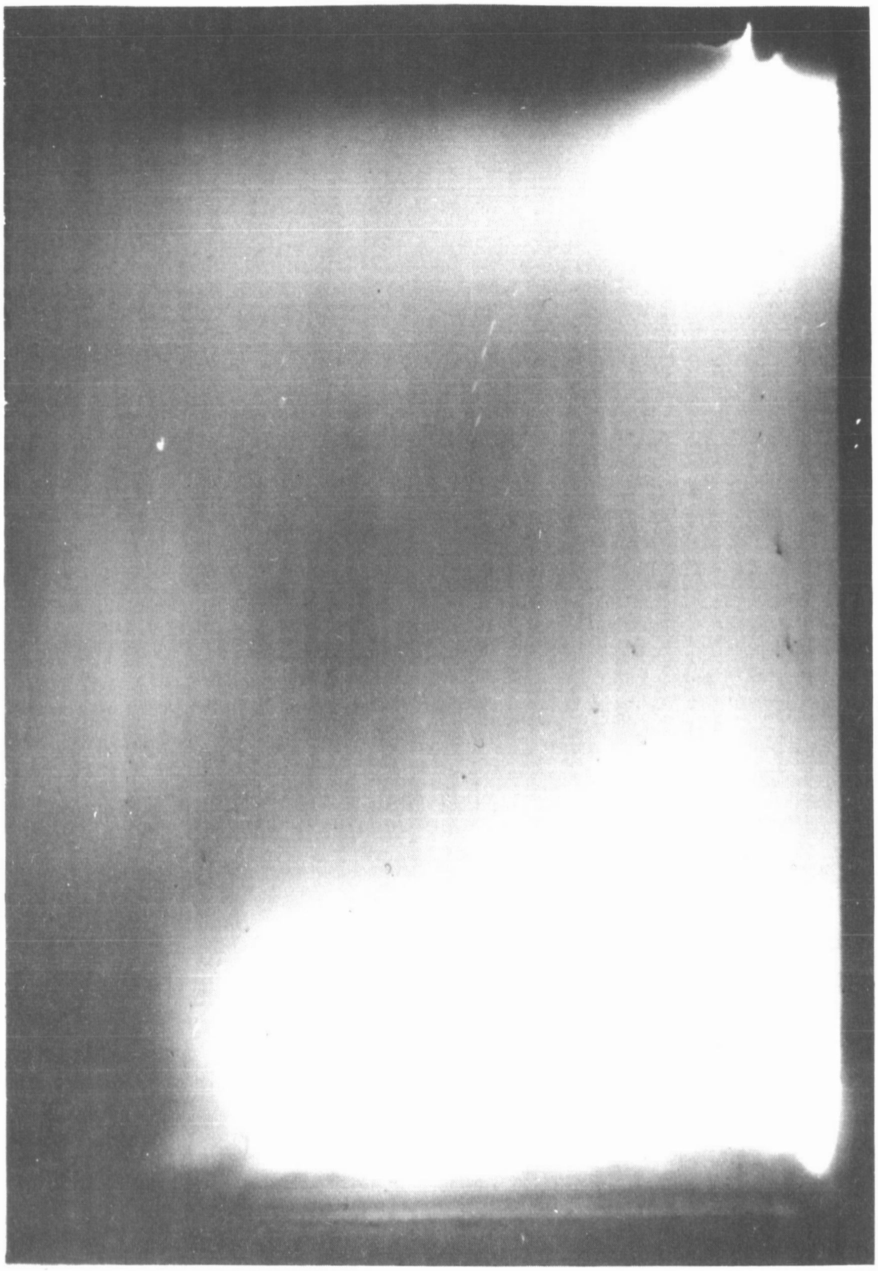

Figure 5. IFP photograph, postbreakdown discharge.

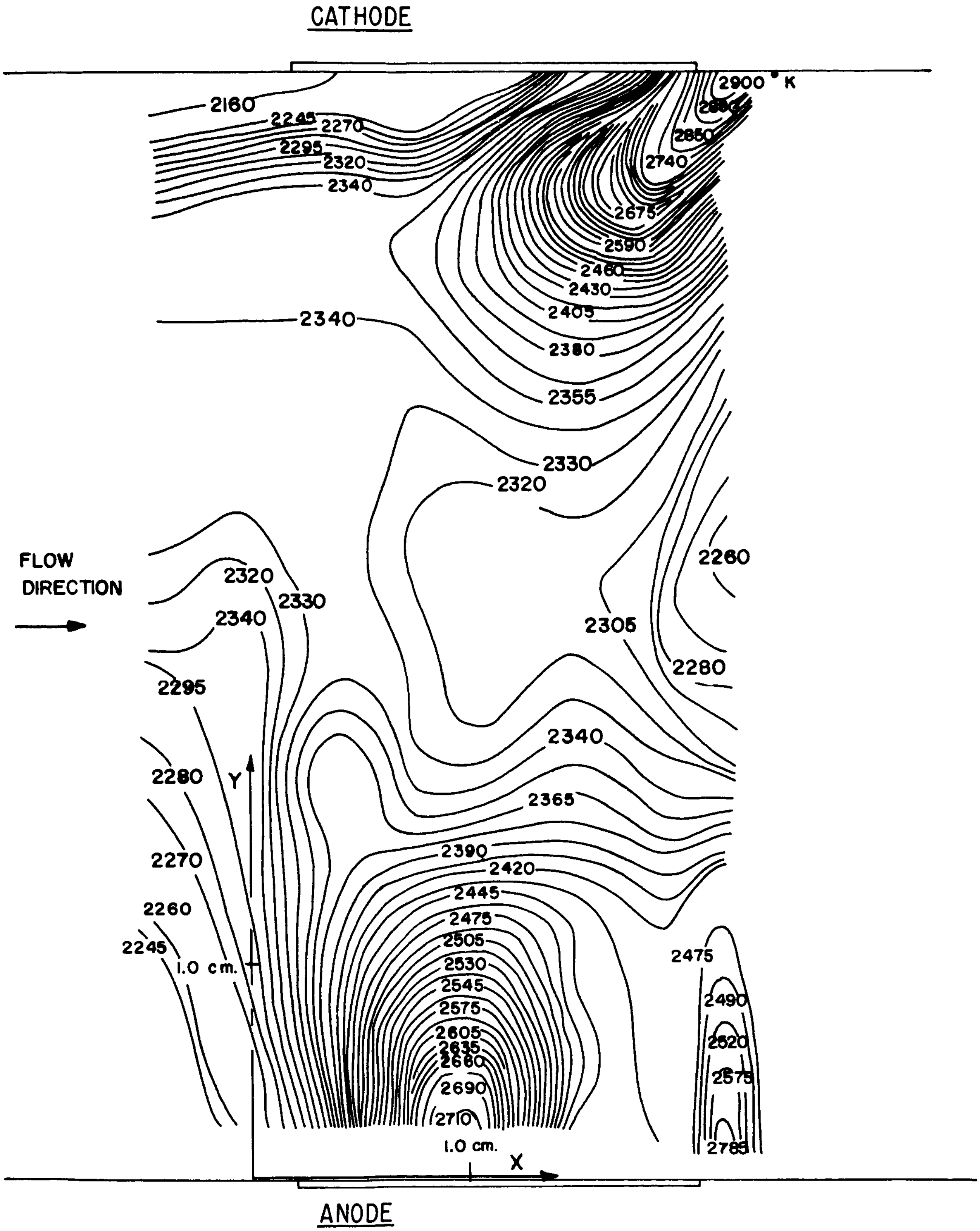

$T_e^{ref} = 2260\ ^\circ K$

I= 4.90 AMPERES, V= 104 VOLTS, λ=5890 Å

Figure 6. Temperature contours, postbreakdown discharge.

where K and K^+ represent the seed atom and ion respectively. The rate equation is therefore

$$\frac{dn_e}{dt} = -\alpha(n_e^3 - K_c\, n_e\, n_K)$$

where α is a recombination rate coefficient and K_c is the equilibrium constant. This equation, with the electron conservation equation, results in an equation for the electron number density profile, of the form

$$\frac{d\beta}{dM} = \underset{\text{(recombination)}}{-Af(M,\gamma,r)\beta^3} + \underset{\text{(ionization)}}{Bg(M,\gamma,r)\beta(1-\beta)e^{-h(M,T_o,V_i)}} \qquad (1)$$

where β is the degree of ionization, M is the Mach number, γ is the specific heat ratio, r is the power of the temperature, V_i is the ionization potential of the seed, and A and B are constants.

An approximate solution to this equation may be obtained by assuming that

$$\beta(M) = \begin{cases} \beta_*(M) & \text{for} \quad M \leq M_F \\ B_F(M) & \text{for} \quad M \geq M_F \end{cases}$$

where $\beta_*(M)$ is the known equilibrium degree of ionization and $B_F(M)$ is the degree of ionization obtained by solving Eq. (1) with $B = 0$, that is, for pure recombination. Following Bray [17] the value for M_F is found by equating the rate of change of the equilibrium degree of ionization to the rate of change of the degree of ionization due only to recombination. It can be shown that this approximate solution is a lower bound to the exact solution and therefore provides a conservative estimate of the degree of ionization.

The results of this solution, for a stagnation temperature of 2000°K, are shown in Figure 7, which presents the electron number density and electrical conductivity as a function of the local argon Mach number. The recombination rate coefficient given by Hinnov and Hirschberg [18] was used

$$\alpha = 5.6 \times 10^{-27}\ T(M)^{-9/2}\ cm^6/sec\ .$$

It can be seen that the electron number density and electrical conductivity freeze out at $M_F = 0.39$, resulting in a conductivity of 9 mho/m at $M = 1.5$.

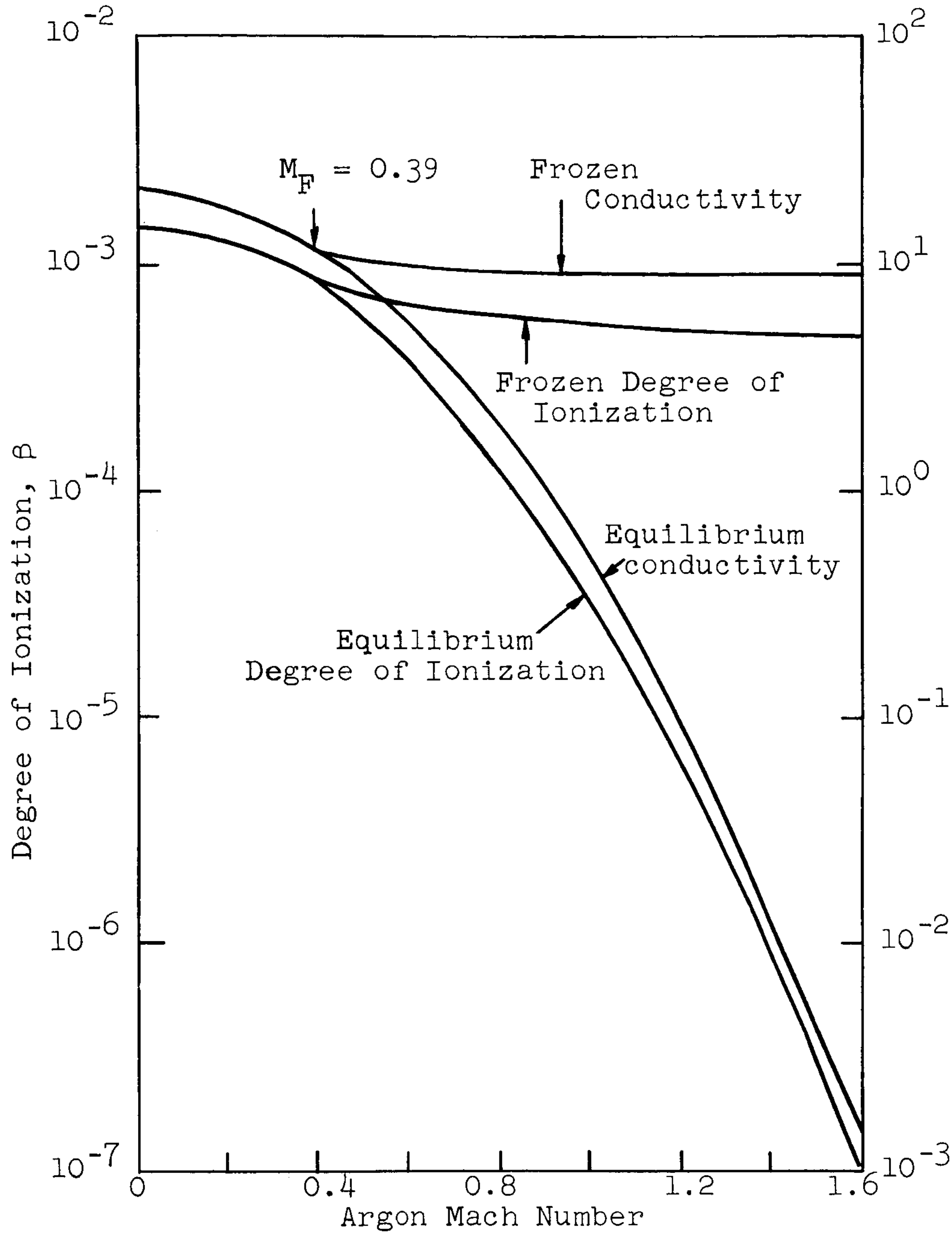

Figure 7. Degree of ionization and electrical conductivity of an argon-cesium plasma as a function of argon Mach number, for a stagnation temperature of 2000°K, stagnation pressure of 15 psig, and 0.2 percent by weight cesium seed.

Microwave Measurements

In order to test these calculations, experiments were undertaken to measure the electron number density using microwaves [19]. Prior to the completion of the seeded argon plasma facility, preliminary experiments were conducted using a seeded combustion gas expanding through a converging-diverging nozzle into the atmosphere, in the form of a free jet. This jet passed between a pair of water-cooled microwave horns located several inches downstream of the nozzle exit. A crystal detector was used to measure the attenuation of two different frequency R-band (8-mm wavelength) microwave signals as they passed through the plasma. From these measurements the electron number density and collision frequency were obtained. Although the measured electron number density and collision frequency agreed with the predicted values to within a factor of two, the presence of the nonequilibrium effect could not be observed primarily because of the difficulty in achieving a shock-free jet at a Mach number of 1.5 and the very low value of the specific heat ratio of the combustion gas. In addition, uncertainties in determining the stagnation gas temperature due to transient heating of the plenum bricks prevented an accurate estimation of the stagnation electron number density.

As a result of these tests, it was concluded that the use of microwaves as a diagnostic tool could enable measurements of the electron number density and electron conductivity to at least within a factor of two. It was also concluded that simultaneous microwave measurements should be made upstream and downstream of the nozzle to eliminate the uncertainty in estimating the stagnation electron number density from gas temperature measurements. Finally, it was decided that measurements should be made in a channel, as opposed to a free jet, so as to better represent the actual configuration of an argon plasma MGD generator, and to enhance the possibility of achieving higher Mach numbers.

The main objective of the experimental program has therefore been to measure the electron number density and electron conductivity at both stagnation and exit locations using a seeded argon plasma. In order to make the measurement, special side plates were designed for an existing test-section housing. One of these plates is shown in Figure 8. The converging-diverging nozzle is located between the two ports which house the microwave horns. Figure 9 shows the test section bricking with the nozzle section.

Since the magnesium-oxide ceramic which normally forms the flow channel is a good dielectric material, it was decided to transmit the microwave signal through the MgO as well as the plasma. Figure 10 shows the arrangement of the microwave horns and the plasma channel. It was found that at certain

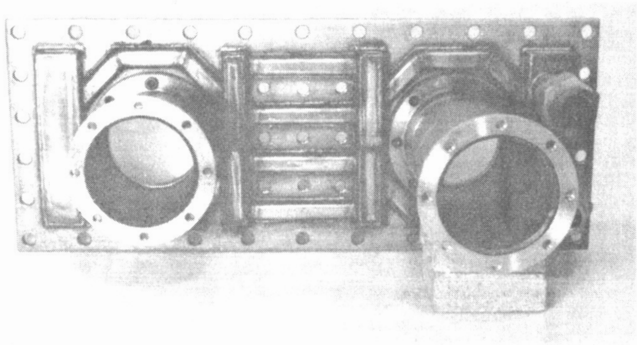

Figure 8. Photograph of side plate showing upstream and downstream microwave ports.

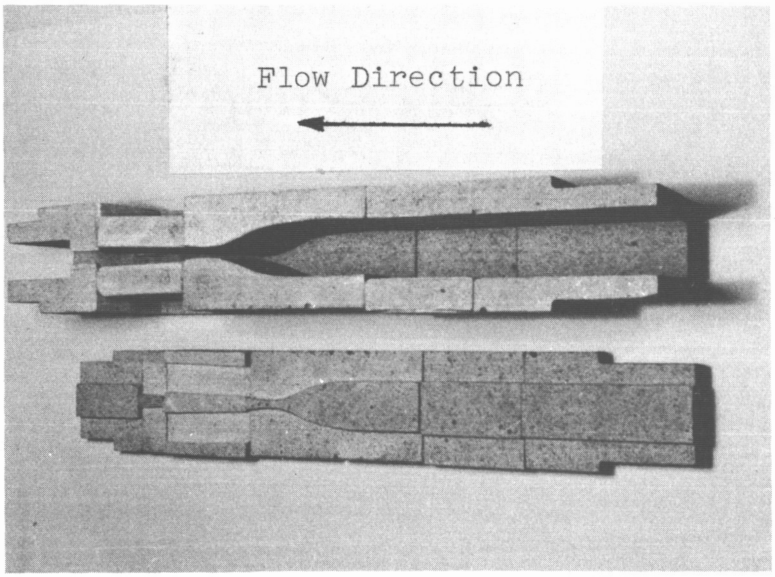

Figure 9. Photograph of MgO test section channel showing supersonic nozzle and microwave window bricks.

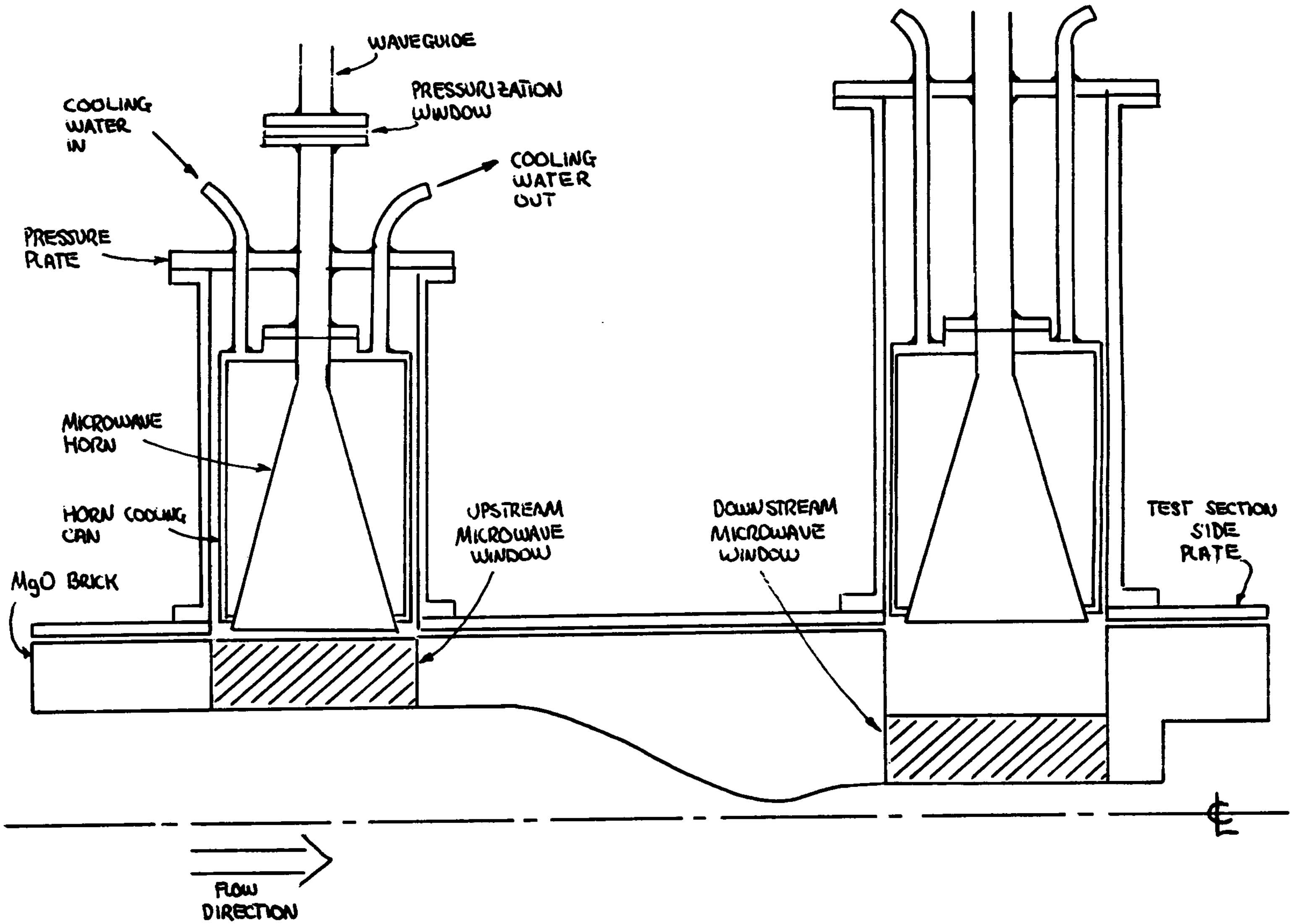

Figure 10. Schematic of test section showing arrangement of microwave horns and windows.

signal frequencies within the X-band (3-cm wavelength) used, the reflection from the ceramic windows, without plasma, is almost zero, and the transmission is accordingly almost complete. Hence, at these frequencies the influence of the MgO windows was negligible, and it was at these critical frequencies that the interferometer measurements were made. The interferometer measurements involved the comparison of the attenuation and phase shift of the microwave signal passing through the plasma to that of a reference signal. The electron number density and collision frequency are then obtained from the attenuation and phase-shift data using theory developed for an idealized model of the propagation of an electromagnetic wave through a plasma [20].

Since the electrical properties of the MgO change with temperature, the critical frequencies drift as the ceramic system heats up. It was therefore necessary to use a swept frequency source to follow these critical frequencies during the course of the test.

A microwave diagnostic technique alternative to the interferometer is that of measuring the attenuation of two microwave signals at different frequencies. The electron number density and collision frequency are then obtained from the two attenuation measurements using the same idealized theory as was used to reduce the interferometer data.

The following flow conditions were typical of the tests conducted:

Subsonic Flow

Nozzle-throat dimension	3.0" x 0.31"
Argon mass flow rate	0.08 lbm/sec
NaK seed fraction	0.001 by weight
Inlet stagnation temperature	1950°K
Plenum pressure	1.0 atmospheres
Upstream location Mach number	0.06
Downstream location Mach number	0.14

Supersonic Flow

Argon mass flow rate	0.35 lbm/sec
NaK seed fraction	0.001 by weight
Inlet stagnation temperature	1950°K
Plenum pressure	1.95 atmospheres
Upstream location Mach number	0.14
Downstream location Mach number	1.05

Figures 11 and 12 are typical of the attenuation data taken at two of the critical frequencies located using the swept-signal generator. Figure 11 shows the reflected and

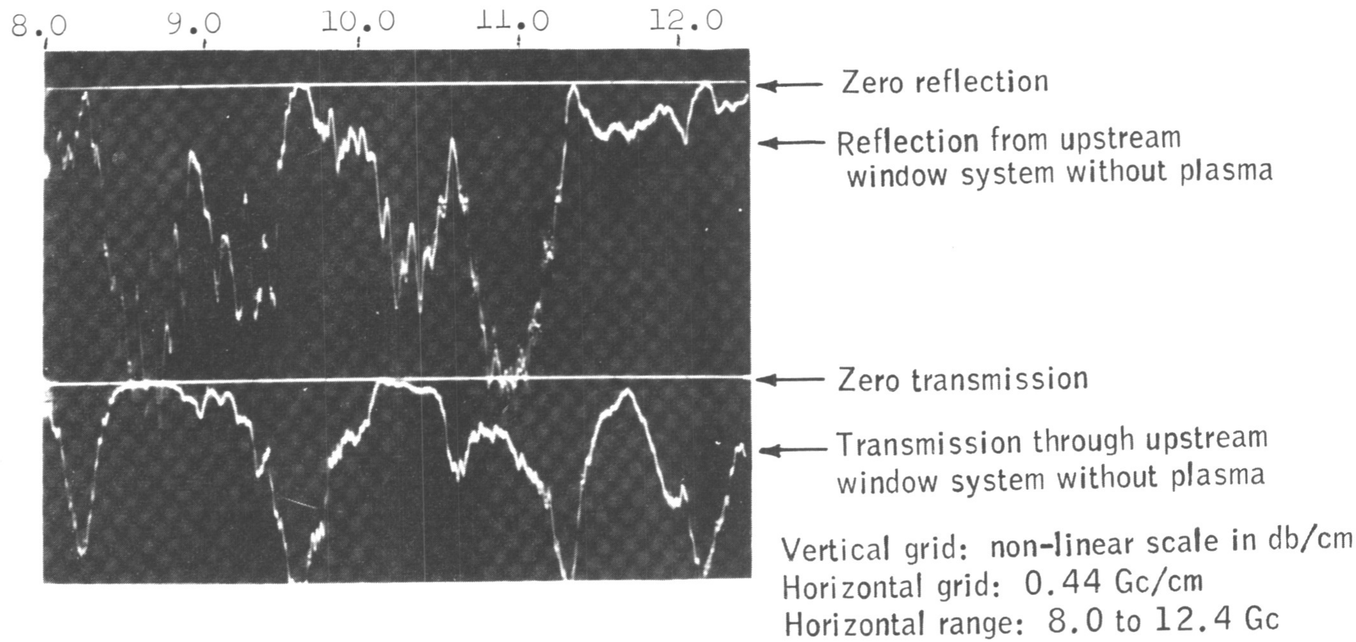

Figure 11. Reflected and transmitted signal strength through upstream window system prior to injection of seed material into hot argon flow, as a function of signal frequency. Note a critical frequency at approximately 9.8 Gc.

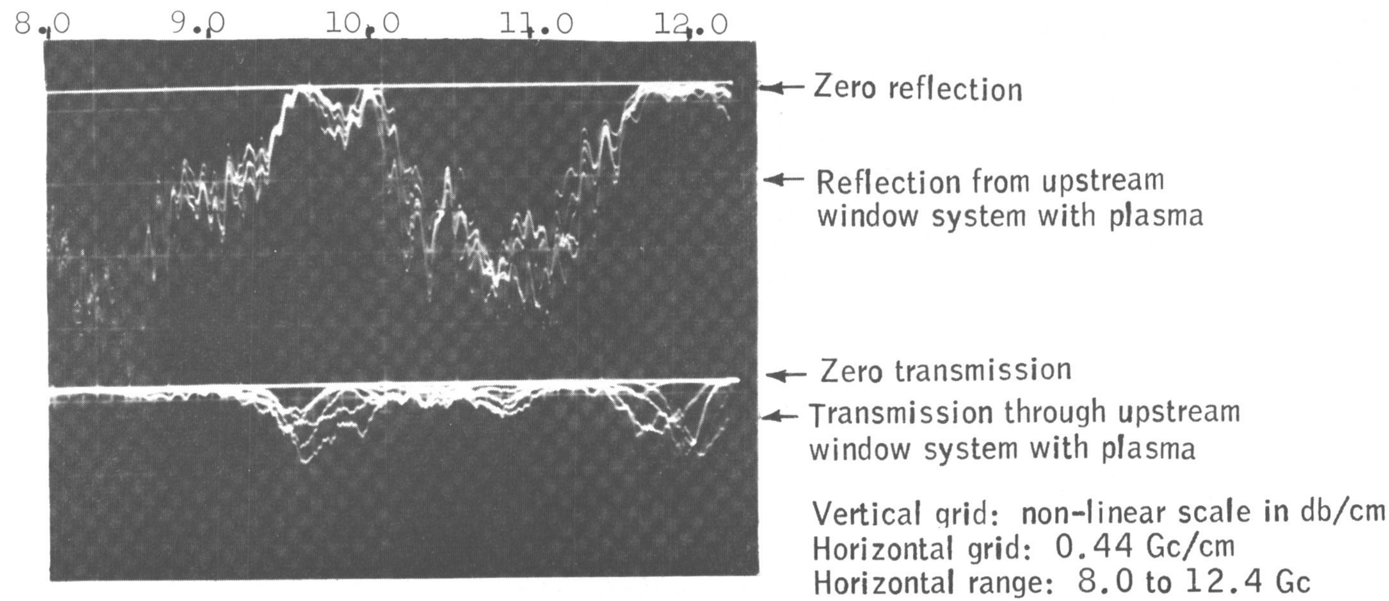

Figure 12. Reflected signal strength through upstream window system with plasma as a function of signal frequency. Note a critical frequency at approximately 9.8 Gc.

transmitted signals at the upstream window before the seed was injected into the hot argon flow. The two critical frequencies are at 9.8 Gc and 12.1 Gc, and it is at one or both of these frequencies that the interferometer data were taken. Figure 12 shows the reflected and transmitted signals in the presence of plasma in the system. The average increase in attenuation of the signal transmitted at these two frequencies was obtained from data such as this.

Using the previously mentioned idealized theory to relate the measured attenuation and phase-shift data to the electron number density and collision frequency, a comparison between the measured and predicted electron number density was made. This comparison is shown in Figure 13 for a typical test condition.

From comparisons such as the one shown in Figure 13, the following conclusions were made:

(1) The measured electron number density at the exit of the nozzle was significantly above the local Saha equilibrium value. The agreement between the measured and predicted electron number densities is reasonably good. The results indicate that there is no faster recombination process than three-body recombination acting under the range of conditions covered in these tests.

(2) The use of a swept-signal generator makes it feasible to use the ceramic channel walls as microwave windows and to locate and operate at those critical frequencies where the windows have negligible effect. The swept-signal method developed for these tests provides data via two techniques: the interferometer and the attenuation at two frequencies. The interpretation of the microwave data so obtained using the idealized theory was verified by making plasma-temperature measurements in the upstream equilibrium region.

A complete report of the work summarized in this section is in preparation. Additional information appears in References 8, 9, and 12.

3.3 <u>Current and Voltage Measurements in a Noble-Gas MHD Generator</u>

3.31 <u>Experimental Apparatus</u>

An open-system arc-heated argon and helium apparatus was constructed which permitted test-section gas temperatures up to 2000°K at both subsonic and supersonic velocities. Run times at test conditions as long as thirty minutes were possible after a preheat period of about fifteen minutes.

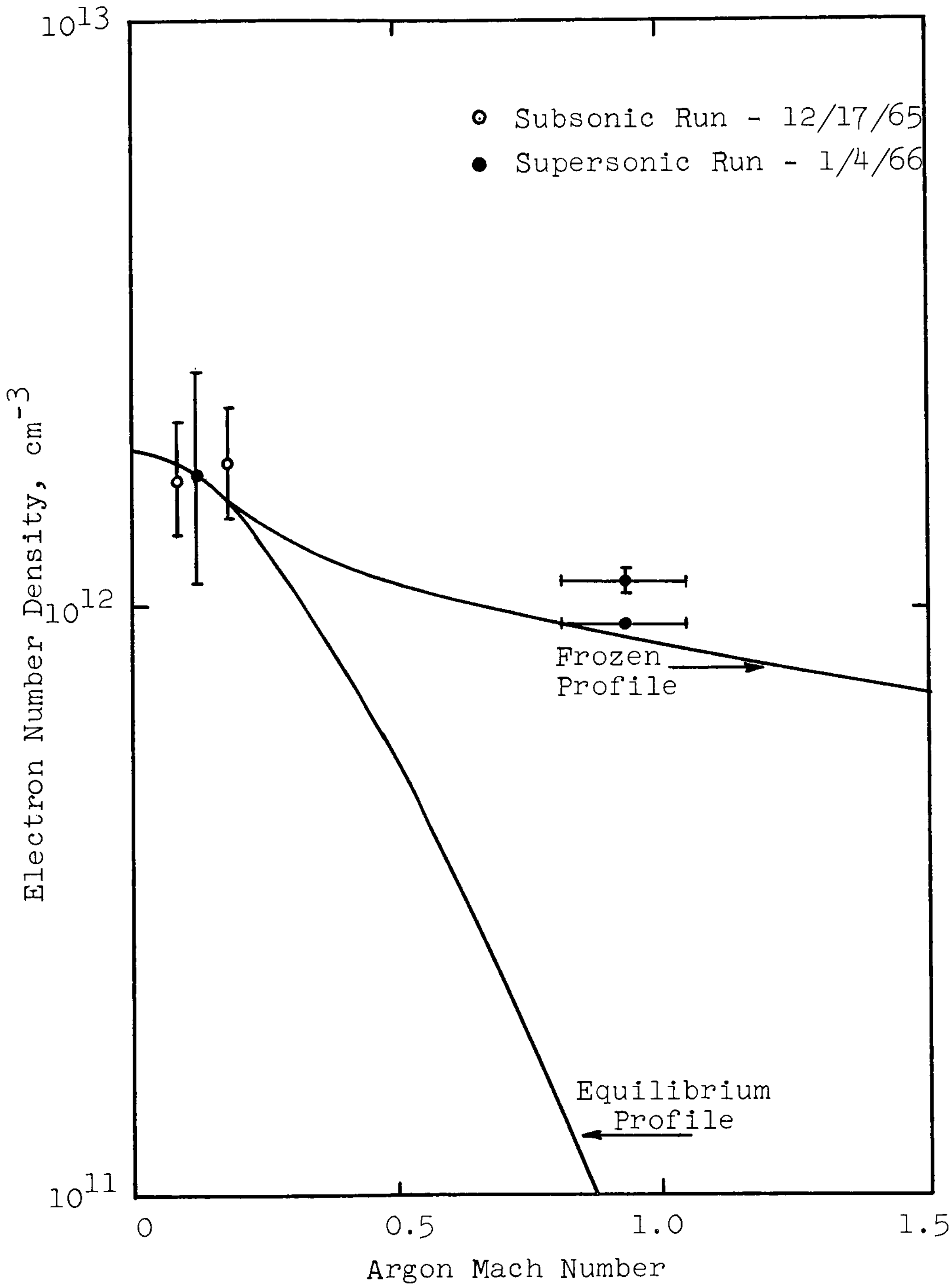

Figure 13. Electron Number Density as a Function of the Argon Mach Number for a 0.1% NaK Seeded Argon Plasma at 1900°K and 1.95 Atmospheres Stagnation Condition.

The apparatus as shown schematically in Figure 14 and in the photograph of Figure 15 is discussed fully in the Quarterly Reports [9,10,11,12]. It consisted of a Thermal Dynamics F-5000 argon arc heater which discharged into a mixing chamber where diluent gas, argon or helium, was added for temperature and composition control. After mixing, the gas flowed through a baffle into a plenum chamber where NaK seed was sprayed into the stream. The residence time in the mixing and plenum chamber was about 10^{-2} second so that thermal equilibrium was achieved before the test section.

Two test sections were used--one with several modifications. The first test section, made of magnesium-oxide ceramic, was designed with a supersonic nozzle for Mach 1.5. After testing it was decided to use a more flexible boron-nitride construction and to operate at subsonic velocities. Supersonic tests were to be resumed after difficulties with deposits and wall electrical leakage were overcome.

The boron-nitride test section proved reliable although considerable difficulty was experienced with a deposit, black or gray in color, which proved conducting at high temperatures. Considerable effort was made to provide a pure gas to the test section, but even during the last test on October 12, 1966, a deposit identified to be largely tungsten and tungsten-boride was found. The deposit problem should not be underestimated as the difficulty in obtaining definitive noble-gas MHD generator performance for low Hall coefficient has been largely due to this effect.

As described in Section 3.33, several MHD generator tests were made with different diagnostic equipment, different electrode configurations, and with different generator conditions.

3.32 Instrumentation

The instrumentation used in the MHD generator part of the program included microwave, spectroscopic, and probe instruments in addition to those used for the usual flow, temperature, and pressure measurements. The conductivity in the plenum chamber before entering the test section was inferred from microwave measurements as described in Section 3.2 and from a four-point probe technique. Representative measured values are compared to calculated values in Table I.

Spectroscopic techniques were developed for measuring the electron temperature which could in turn be related to the current density through the electron energy equation. This method is reported in Section 3.1. An optical sapphire window was used in some MHD generator experiments, and a slot was used in others when it was found that the sapphire window

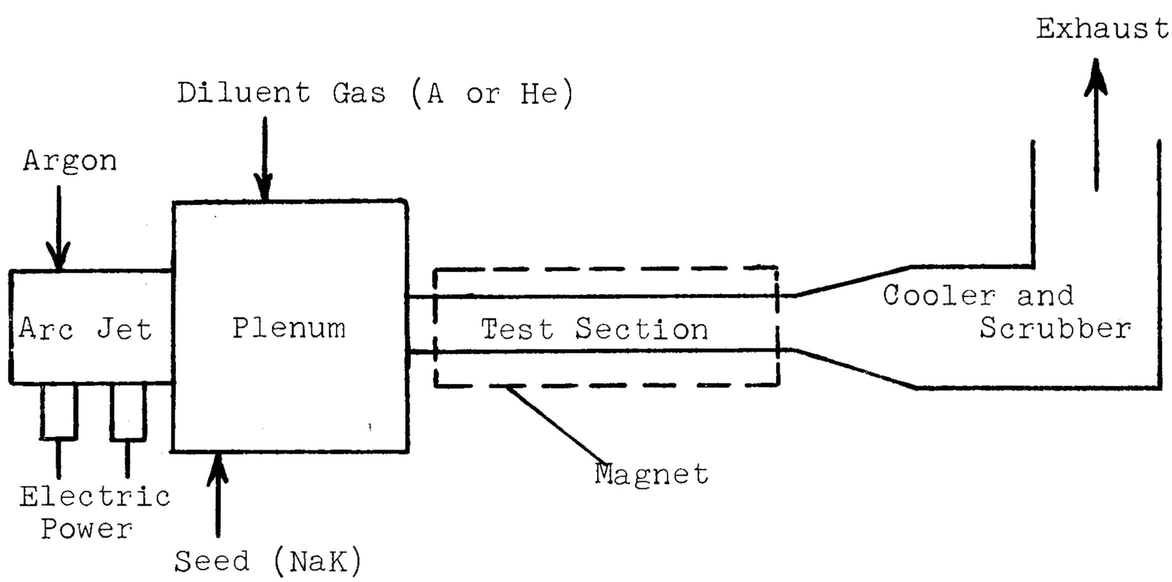

Figure 14. Schematic Diagram of
Experimental Facility.

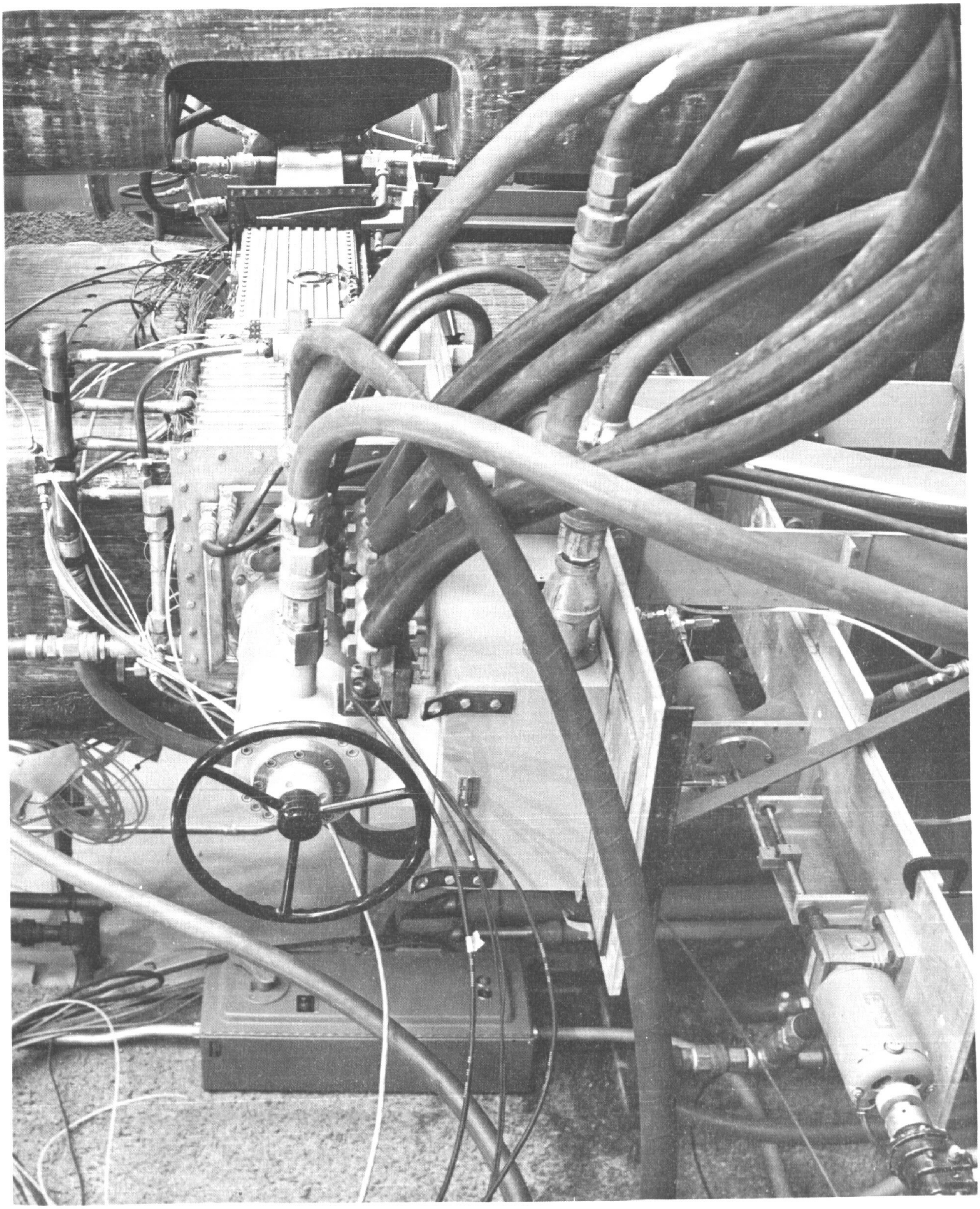

Figure 15. Arc heater, plenum, and test channel installed in magnet.

TABLE I

ELECTRICAL CONDUCTIVITY MEASUREMENTS
(Argon with 0.1 per cent NaK seed)

Average Temperature, ^{o}K	σ_{calc}, mho/m	$\sigma_{measured}$, mho/m	Method
1605	3×10^{-1}	3.5×10^{-1}	Four-point probe
2060	12	29	Four-point probe
2070	13	35	Four-point probe
1950	6	6^{*}	Microwave

*This measured conductivity was calculated from the microwave measurement of $n_e \approx 2 \times 10^{12}\ cm^{-3}$.

became somewhat opaque due to deposits. IFP electron temperature measurements were made with applied electric field and with applied magnetic field. In no MHD generator experiment, however, were currents of sufficient magnitude developed to make the current distribution observable. The technique is now available, but noble-gas MHD generator performance must be improved before current distribution measurements are possible.

Gas temperatures were measured by tungsten, tungsten-rhenium thermocouples which were often used also as electric field probes. Because of internal shorting along the walls, the probe data were not meaningful. In addition, numerous tungsten wire probes were used to measure the electric field between cathode and anode and also in the Hall direction. Electrode temperatures were measured by thermocouples mounted through hollow electrode stems and attached to the back surface of the electrodes.

Pressure measurements in connection with mass flow rates and gas temperature were used to infer gas velocity and Mach number. The flow reached a Mach number of 1.5 for the supersonic test, but most runs were made at a Mach number of about 0.5.

3.33 Power-Generation Results

Four power-generation experiments were made during the contract period* although many preliminary experiments for other purposes, such as spectroscopic investigations, were conducted. The detailed results are given in the Quarterly Progress Reports [10,11,13,14], and are summarized below in Table II.

Since the theoretical open-circuit voltage for all runs exceeded 30 volts and the short-circuit current per electrode calculated from simple theory exceeded the measured value by several times, it is clear that the generator performance was seriously degraded. Wall resistance measurements made before and after the test period while the walls were at the same temperature as during the test showed a serious decrease in resistance. Inspection after the experiment showed a deposit on the walls which may have been the cause for shorting both axially and in the u x B direction. The consequences of wall short circuits and conductivity nonuniformities on generator performance are described in the following section.

3.34 Effect of Wall Leakage and Conductivity Nonuniformity on MHD Generator Performance

In the limit in which the electrode structure of a linear magnetohydrodynamic generator becomes either infinitely finely segmented or continuous, nonuniformities resulting from the finite size of electrode segments vanish. If in addition property variations occur only the y-direction as shown in Figure 16, then all x-direction nonuniformities vanish. In this limit of one-dimensional nonuniformities, Rosa [21] has obtained solutions to the electrical equations. His results may be case in the form of a "global" Ohm's law for a nonuniform gas. Let V_x' represent the axial voltage difference in a generator over the axial length ℓ, and let V_y' represent the transverse voltage difference across the generator in height h measured in the reference frame of the moving gas $[V_y' = V_y + B \int_0^h u(\xi)d\xi;\ V_x' = V_x$ where V_y and V_x are the transverse and axial voltages measured in the laboratory frame]. The total current flowing in the transverse direction across length ℓ per unit depth of channel is denoted I_y, and the net axial current flowing in the channel across the height h is denoted I_x. Rosa's results may be represented in terms of the vectors $\vec{V}(V_x',V_y')$ and $\vec{I}(I_x,I_y)$ as

$$\vec{V}' = \overleftrightarrow{R}\cdot\vec{I}, \quad \vec{I} = \overleftrightarrow{S}\cdot\vec{V}', \qquad (2)$$

where R_1 is the resistance tensor of the generator and $\overleftrightarrow{S} = (\overleftrightarrow{R})^{-1}$ is the conductance tensor:

*Most preparations for the last experiment on October 12, 1966 were made during the contract period although the experiment was run after the conclusion of the contract period.

TABLE II

Test Date	$V_{oc,max}$ volts	$I_{sc,max}$ amps per electrode	x	B	$\omega\tau$	$\sigma_{\mathrm{¢}}$	$T_{\mathrm{¢}}$, °K	M	$\frac{He}{A}$	Remarks
7/23/65	2.5	.026	.005	.56	2.5	8.3	2000	1.5	0	MgO test section, 14 electrode pairs.
1/31/66	11.5	.00025	.007	2.0	7.5	.56	1650	.48	0	BN test section, 7 electrode pairs.
6/15/66	12	.007	.017	1.0	1.8	1.5	1900	.50	2	BN test section, 15 electrode pairs.
10/12/66	2.1	.042	.02	1.0	1.4	2.3	1950	.45	2	Same as above except 2 electrode pairs were pins.

In the above table the symbols are defined as the following:

x = molar potassium seeding fraction

B = magnetic induction in Tesla

$\omega\tau$ = Hall parameter

$\sigma_{\mathrm{¢}}$ = calculated electrical conductivity at channel centerline in mho per meter

$T_{\mathrm{¢}}$ = temperature at channel centerline

M = Mach number

He/A = helium to argon atomic ratio in mixture

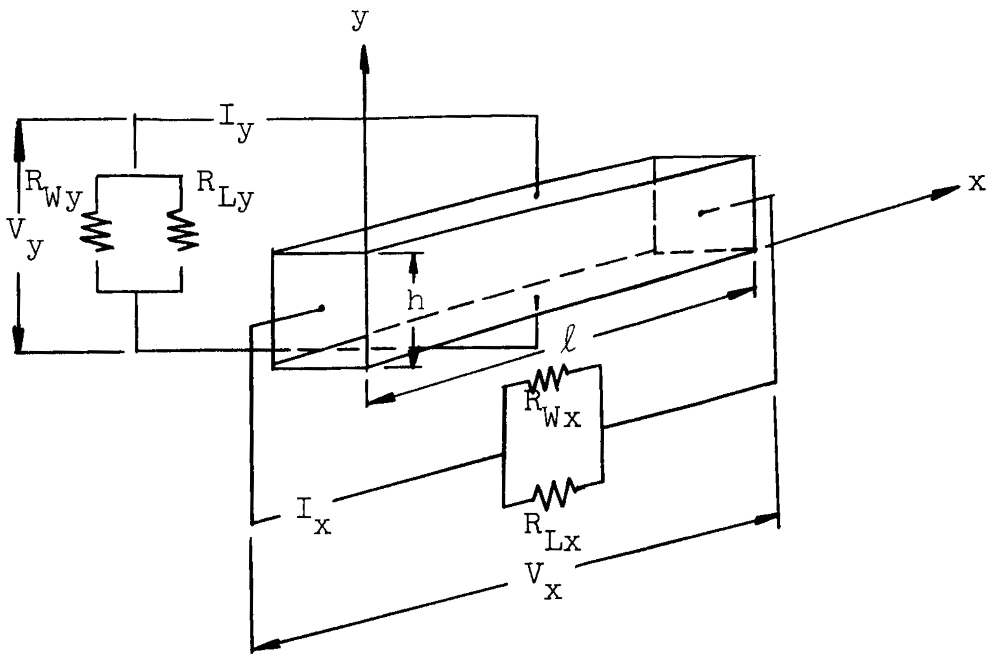

Figure 16

$$\overleftrightarrow{R} = \frac{R_y(0)}{\langle\sigma\rangle\langle\sigma^{-1}\rangle}\begin{pmatrix}(\frac{\ell}{h})^2 & -\langle\beta\rangle\frac{\ell}{h} \\ \langle\beta\rangle\frac{\ell}{h} & G\end{pmatrix}, \tag{3}$$

$$\overleftrightarrow{S} = \frac{R_y^{-1}(0)\langle\sigma^{-1}\rangle}{\langle\frac{1+\beta^2}{\sigma}\rangle}\begin{pmatrix}G(\frac{h}{\ell})^2 & \langle\beta\rangle\frac{h}{\ell} \\ -\langle\beta\rangle\frac{h}{\ell} & 1\end{pmatrix}. \tag{4}$$

The transverse impedance of the gas in the absence of a magnetic field is $R_y(0) = \langle\frac{1}{\sigma}\rangle \frac{h}{\ell}$ and

$$G = \langle\sigma\rangle\langle\sigma^{-1}\rangle [1 + \langle\sigma^{-1}\rangle^{-1} (\langle\beta^2\sigma^{-1}\rangle - \langle\beta\rangle^2\langle\sigma\rangle^{-1})] \tag{5}$$

contains the coupling of nonuniformities and the Hall effect and is equal to unity in a uniform gas. The average $\langle\ \rangle$ of any function f(y) is defined as

$$\langle f(y)\rangle = \frac{1}{h}\int_0^h f(y)dy\ . \tag{6}$$

We shall now apply the foregoing results to the generator with wall leakage to obtain the coupled effects of such leakage combined with conductivity nonuniformities. The transverse voltage V_y and axial voltage V_x of a magnetohydrodynamic generator of length ℓ and height h may be related to the transverse and axial currents I_y, I_x by the external impedances impressed upon the generator:

$$V_x = I_x R_x \quad ,$$
$$V_y = I_y R_y \quad . \tag{7}$$

The impedance R_x represents the equivalent resistance of the load and wall leakage for the axial circuit, and R_y represents the equivalent resistance of the load and wall leakage for the transverse circuit. Let the wall leakage impedances in the axial and transverse directions be denoted by R_{Wx}, R_{Wy} respectively, and let the corresponding load resistances be denoted R_{Lx}, R_{Ly}. Since the wall leakage is in parallel with the load for either circuit, we have

$$R_x = \frac{R_{Lx}R_{Wx}}{R_{Lx}+R_{Wx}} \quad , \quad R_y = \frac{R_{Ly}R_{Wy}}{R_{Ly}+R_{Wy}} \quad . \tag{8}$$

The global Ohm's Law for the gas from (2) is

$$V_x = I_x R_{pxx} + I_y R_{pxy}$$
$$V_y + \langle uB \rangle h = I_x R_{pyx} + I_y R_{pyy} \tag{9}$$

where

$$R_{pxx} = R_x(0)/\langle\sigma\rangle\langle\sigma^{-1}\rangle \quad , \quad R_{pxy} = -\langle\beta\rangle\frac{\ell}{h}R_y(0)/\langle\sigma\rangle\langle\sigma^{-1}\rangle \quad ,$$

$$R_{pyx} = \langle\beta\rangle\frac{\ell}{h}R_y(0)/\langle\sigma\rangle\langle\sigma^{-1}\rangle \quad , \quad R_{pyy} = G\, R_y(0)/\langle\sigma\rangle\langle\sigma^{-1}\rangle \quad , \tag{10}$$

and $R_x(0) = (\frac{\ell}{h})^2 R_y(0)$. Substituting from (7) into (10) we find

$$-V_x = \frac{\langle\beta\rangle\langle uB\rangle \ell\theta R_y(0) R_x}{R_x(0) R_y [G + \frac{R_y(0)}{R_y\langle\sigma\rangle\langle\sigma^{-1}\rangle} (1+\theta\langle\beta\rangle^2)]} \quad , \tag{11}$$

$$-V_y = \frac{\langle uB\rangle h}{1 + \frac{R_y(0)}{R_y\langle\sigma\rangle\langle\sigma^{-1}\rangle} (G + \theta\langle\beta\rangle^2)} \quad , \tag{12}$$

where

$$\theta \equiv \frac{R_{pxx}}{R_{pxx} + R_x} \quad . \tag{13}$$

In a uniform gas, $G = 1$ and the effect of nonuniformities is to make $G > 1$. Nonuniformities can be seen to further degrade the already degraded performance of the generator with wall leakage effects.

When β is uniform, G reduces to the form

$$G = 1 + G^*(1+\beta^2) \ , \tag{14}$$

where $G^* = \langle\sigma\rangle\langle\sigma^{-1}\rangle-1$. The voltages V_x, V_y are then

$$-V_x = \frac{\beta\langle uB\rangle\ell\ R_y(0)R_x}{R_x(0)R_y[1+G^*(1+\beta^2) + \dfrac{R_y(0)}{R_y\langle\sigma\rangle\langle\sigma^{-1}\rangle}(1+\theta\beta^2)]} \ , \tag{15}$$

$$-V_y = \frac{\langle uB\rangle h}{1 + \dfrac{R_y(0)}{R_y\langle\sigma\rangle\langle\sigma^{-1}\rangle}[1 + G^* + (\theta+G^*)\beta^2]} \ . \tag{16}$$

To obtain estimates of G*, let us consider the model distribution

$$\sigma(y) = \begin{cases} \sigma_\omega + \frac{y}{\delta}(\sigma_o-\sigma_\omega) & 0 \le y \le \delta \\ \sigma_o & \delta \le y \le h-\delta \\ \sigma_\omega + \frac{(h-\delta)}{\delta}(\sigma_o-\sigma_\omega) & h-\delta \le y \le h \end{cases} \tag{17}$$

which represents the effects of layers of variable conductivity of thickness δ near the electrodes. The conductivity of the core region is σ_o, and the conductivity at the walls (y=0,h) is σ_ω. The factor G* has been calculated for this distribution and is shown in Fig. 17. As an illustration, consider the open-circuit voltage V_y(o.c.) for Faraday operation (R_{Lx}, $R_{Ly} \rightarrow \infty$) calculated according to Eq. (12). We assume, for illustration, that there exist leakage resistances such that $\theta = 0.2$ and $R_y(0)/R_y\langle\sigma\rangle\langle\sigma^{-1}\rangle = 0.2$. If there are no nonuniformities, $G^* = 0$ and

$$-V_y(\text{o.c.}) = \frac{\langle uB\rangle h}{1 + 0.2(1 + 0.2\beta^2)} \ .$$

In particular, for $\beta = 2$,

$$-V_y(\text{o.c.}) \approx .74\langle uB\rangle h \ .$$

Now consider that uniformities also exist. For $\delta/h = 0.2$ and $\sigma_\omega/\sigma_c = 10^{-2}$, we find from Fig. 17 that $G^* \approx 0.6$. Then

$$-V_y(\text{o.c.}) = \frac{\langle uB\rangle h}{1 + 0.2\ (1.6 + 0.8\beta^2)} \ .$$

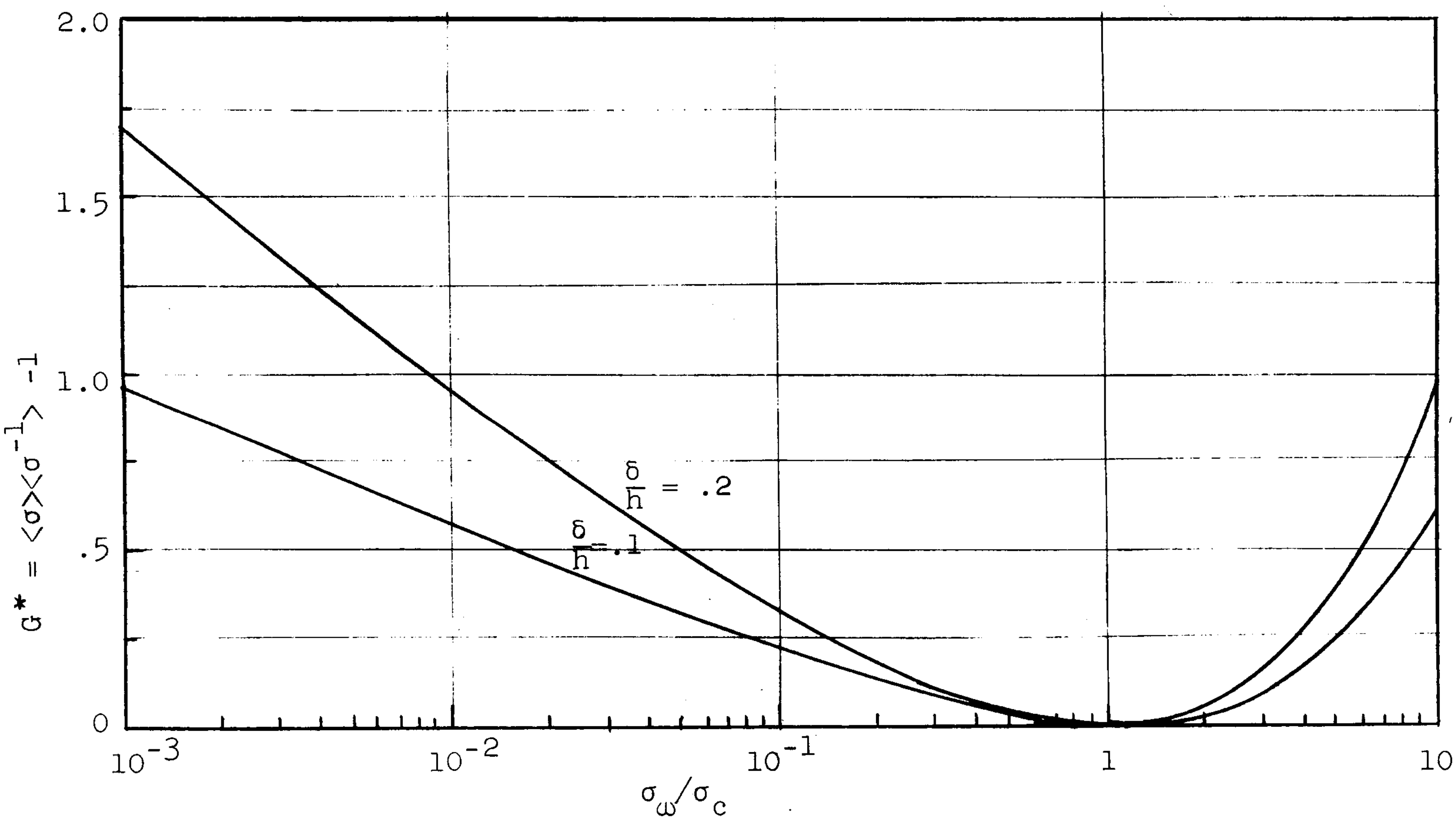

FIGURE 17. Conductivity Nonuniformity Factor G^* for the Model Given by Eq. (17).

For $\beta = 2$, we have from the above

$$-V_y(\text{o.c.}) \approx 0.5 \langle uB \rangle h \quad .$$

We thus find that a significant correction to wall leakage effect calculations can be introduced by electrical conductivity nonuniformities. These values should be compared to the case where there is neither axial leakage nor nonuniformities, in which case $-V_y(\text{o.c.}) = .833 \langle uB \rangle h$. The relative importance of nonuniformities become much more pronounced for larger β.

3.4 Rogowski Coil Experiments

An explorative investigation was conducted to evaluate the feasibility of using a Rogowski coil probe to measure current distributions within the MHD generator channel. Probes of various sizes and configurations were fabricated and measurements were made in a salt solution. Electrode arrangements were varied to provide current patterns in the salt solution which could be calculated or inferred from measurements on electrically conducting paper.

It was found that all probes tested were sensitive to currents outside of the area enclosed by the coil and that signals for current densities of 1 ampere per sq cm were marginal in view of noise and non-uniform magnetic field problems. After initial tests of the MHD generator described above when it became clear that very small current densities would be obtained, it was decided to discontinue work on the Rogowski coil probe. Until larger current densities are observed in noble gas MHD generators, it was not felt appropriate to pursue the considerable development necessary to provide probes suitable for the hot, seeded environment in these generators.

4.0 ANALYTICAL PROGRAM

4.1 Electron Distribution Function in a Nonequipartition Plasma

The accurate prediction of the electron temperature, electrical conductivity, and other properties in a partially ionized nonequipartition plasma rests on a knowledge of the electron distribution function. Of particular interest are the conditions under which departures occur from a Maxwellian form for the isotropic part f^0 of the distribution. To this end the electron Boltzmann equation has been formulated for a spatially uniform, steady-state plasma in a strong electric field, employing an expansion in spherical harmonics and the simplifications consistent with the small electron mass. Boltzmann collision operators were used for electron-neutral and electron-ion collisions, and the Fokker-Planck operator for electron-electron encounters. The heavy-particle distribution functions were assumed to be Maxwellian at the temperature T_h.

In the initial analysis the effects of nonelastic collisions were neglected. The conditions studied and qualitative results can be discussed in terms of the following diagram:

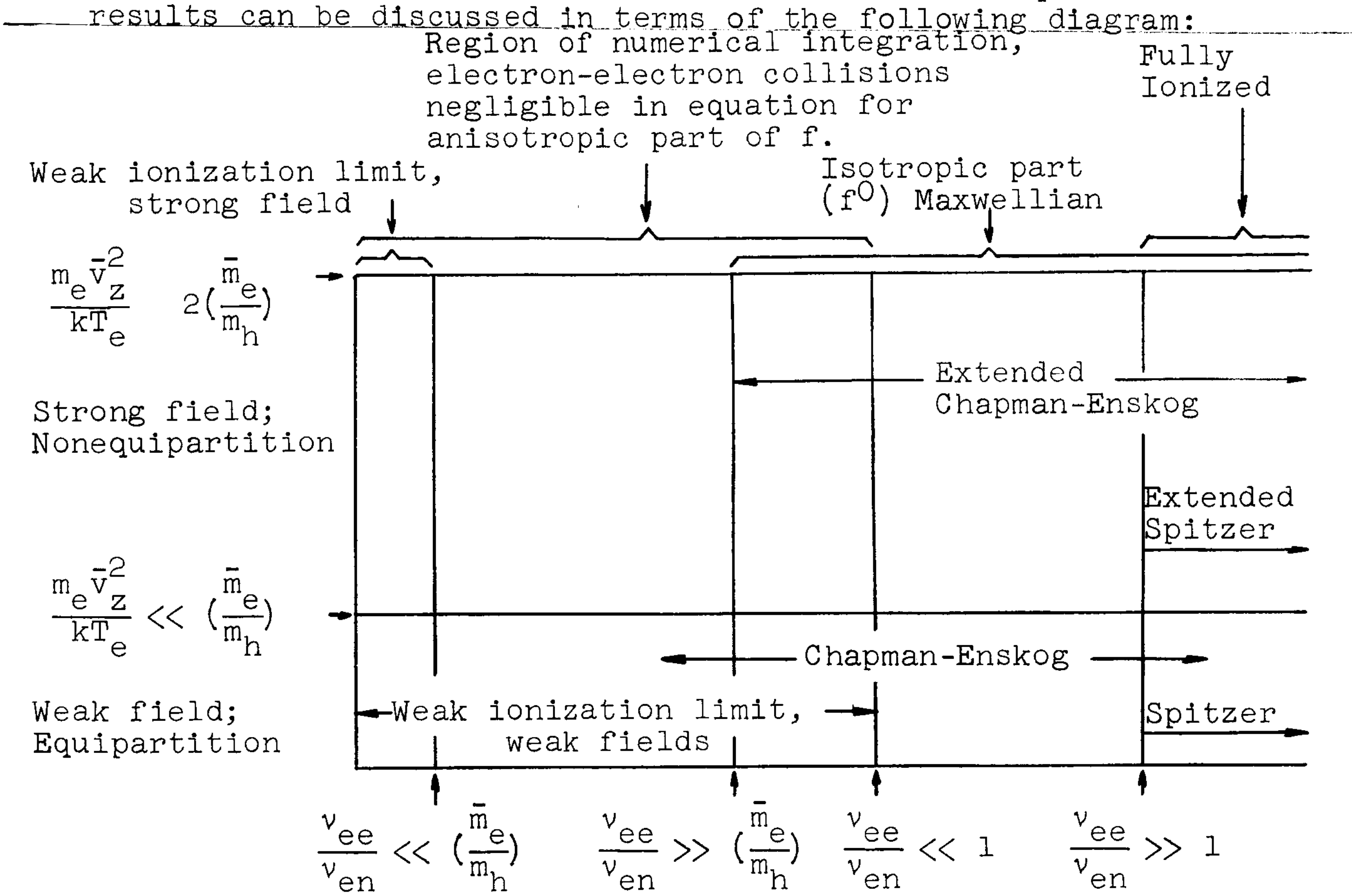

Here the ordinate, the square of the ratio of the electron drift velocity $\bar{v}_z$ to the mean electron thermal speed, is approximately equal to the ratio of the average energy gained by an electron between collisions in an electric field to the electron thermal energy. Hence the ordinate is a measure of the strength of the electric field. The abscissa is the ratio of the electron-electron collision frequency to the total electron-neutral collision frequency and is a measure of the degree of ionization. The upper limit on the diagram corresponds to the static instability referred to by Kerrebrock [22].

Values of the ordinate very much less than the mean electron-to-heavy-particle mass ratio $(\overline{m_e/m_h})$ correspond to weak electric fields where f^0 is Maxwellian and electron and heavy particle temperatures are equal. In this region, the electrical conductivity σ can be calculated accurately by means of the Chapman-Enskog expansion. Spitzer and Härm's [23] results for fully ionized plasmas apply when $\nu_{ee}/\nu_{en} >> 1$, the weak ionization (Lorentz) limit occurs when $\nu_{ee}/\nu_{en} << 1$.

In the nonequipartition case, when $\overline{v_z^2} / \frac{kTe}{m_e} \not\ll (\overline{m_e/m_h})$, the electron temperature $T_e \equiv m_e\overline{v^2}/3k$ can be found from the expression

$$\frac{j_z^2}{\sigma} = \int_0^\infty m_e v^2 \left(\sum_h \frac{m_e}{m_h} n_h Q_h v\right) \left[f^0 + \frac{T_h}{T_e} \left(\frac{kT_e}{m_e v} \frac{df^0}{dv} \right) \right] 4 \pi v^2 dv$$

where $Q_h(v)$ is the cross section for momentum transfer between electrons and the heavy species h, n_h the number density of species h, and j the current density.

It can be shown from an analysis of the kinetic equations that whenever $\nu_{ee}/\nu_{en} >> (\overline{m_e/m_h})$, the isotropic part of the distribution function is Maxwellian, although at an elevated temperature. When this holds the equation for the anisotropic part of the distribution function becomes independent of the heavy-particle temperature. In this limit the Chapman-Enskog solution for the electrical conductivity can be accurately extended to nonequipartition plasmas. That is, in the fully ionized limit Spitzer and Härm's results apply with the electron temperature replacing the gas temperature. Between $\nu_{ee}/\nu_{en} >> (\overline{m_e/m_h})$ and the fully ionized limit the results of Schweitzer and Mitchner [24], which compare the mixture rule of Frost to the Chapman-Enskog solution, can be extended to the strong-field region by the use of T_e in place of T_h.

The transition between the weak-ionization (Lorentz) and Maxwellian forms for f^0 has been studied by numerical integration of the kinetic equations in the region $\nu_{ee}/\nu_{en} << 1$. As indicated in the diagram, this region overlaps the region where f^0 is Maxwellian. Accordingly, it has been possible to demonstrate numerically the transition to an elevated-temperature Maxwellian. Typical results are shown in Figure 18. When $\nu_{ee}/\nu_{en} << 1$ the electron-electron collision terms can be neglected in the equation for the anisotropic part of the distribution function and the electrical conductivity is given by

$$\sigma = \frac{4 \pi e^2}{3m_e} \int_0^\infty \frac{v^2}{\sum_h n_h Q_h} \left(\frac{-df^0}{dv} \right) dv \quad .$$

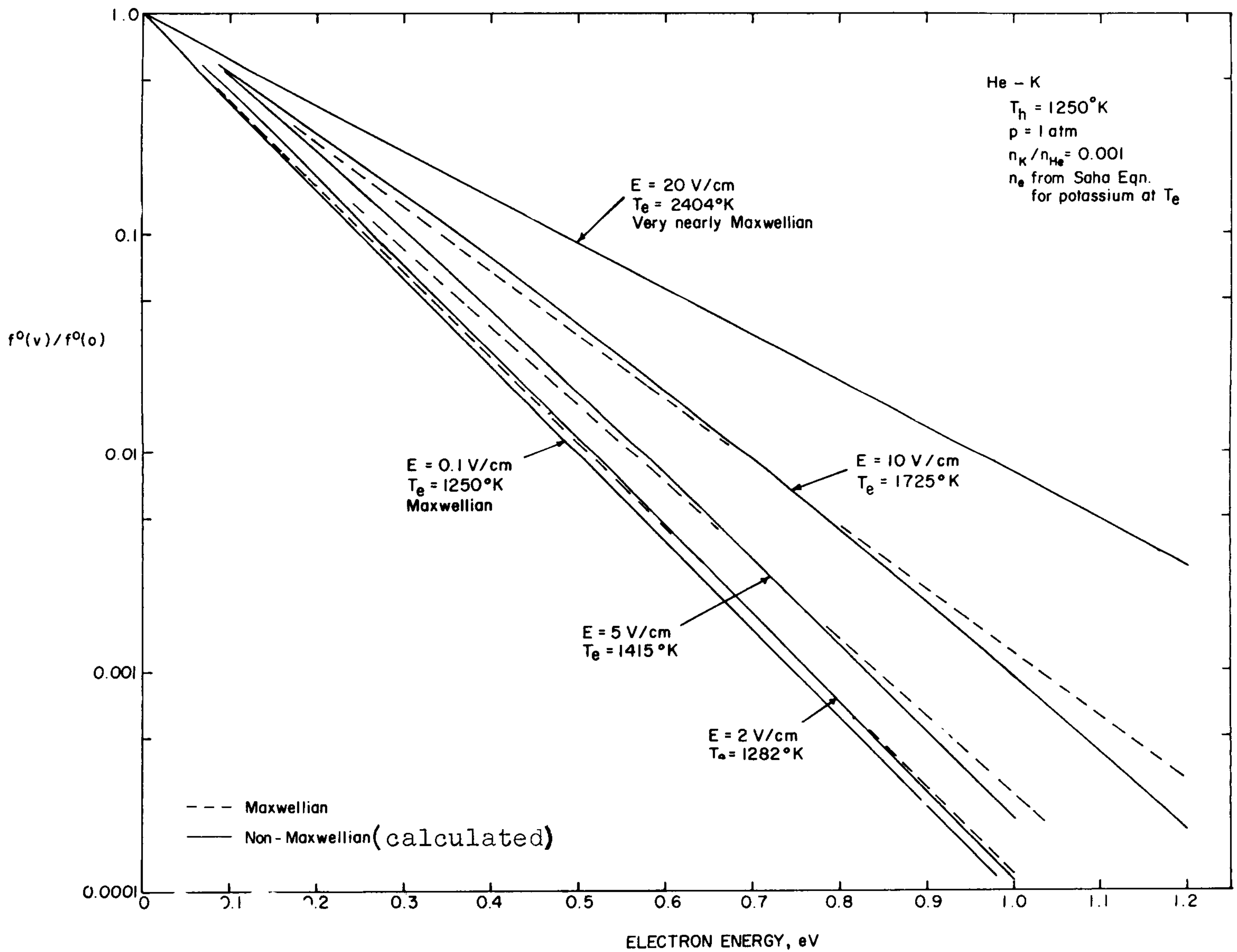

Figure 18. Normalized electron distribution function for various electric-field strengths.

Here, in general, f^0 must be obtained numerically. It has been found, however, that accurate values for σ can be obtained from this equation by the use of a Maxwellian f^0 based on the actual electron temperature from the numerical solution.

Calculated electrical conductivities have been compared with the experimental results of Kerrebrock and Hoffman [25] and Cool and Zukoski [26]. As shown in Figure 19 good agreement with the data was obtained at the higher current densities where the radiative energy loss, which was not considered in the calculations, could be neglected. Under the conditions of these experiments, no significant departures from a Maxwellian f^0 are predicted by the numerical solutions.

In the foregoing analysis, the effects of nonelastic collisions have been neglected. Under certain conditions of interest, however, such collisions will be of importance in the electron Boltzmann equation. Moreover, the electron number density and excited-state populations are determined by a balance between nonelastic collisional processes and radiation escape. The relationship of the electron density to the value given by the Saha equation is of major significance in calculations of the electrical conductivity; the excited-state populations are particularly pertinent to the spectroscopic diagnostic techniques discussed in Section 3.1. These quantities can be found from the solution of the set of rate equations that describe the collisional and radiative rates at which various states are populated and depopulated. Since the rate equations involve the electron distribution function, their solution is coupled with the solution of the electron Boltzmann equation. The analysis described above has been extended to investigate this coupling.

In the rate equations, a three-level model for the seed atom has been considered with the degree of radiation escape adjusted by means of radiation escape coefficients, as in the calculations of Ben-Daniel and Tamor [27]. To date, calculations have been performed for the case of cesium-seeded helium, with nonelastic collisions neglected in the electron Boltzmann equation. The coupling then results from the effect of a non-Maxwellian distribution function in the rate equations and the effect of the degree of ionization on the relative importance of electron-electron collisions in the Boltzmann equation.

The results of the calculation confirm qualitative ideas about deviations from the Saha equation and the expected shape of the distribution function. At low electric fields the distribution function is nearly Maxwellian at the gas temperature. As the electric field is increased, two effects compete for dominance.

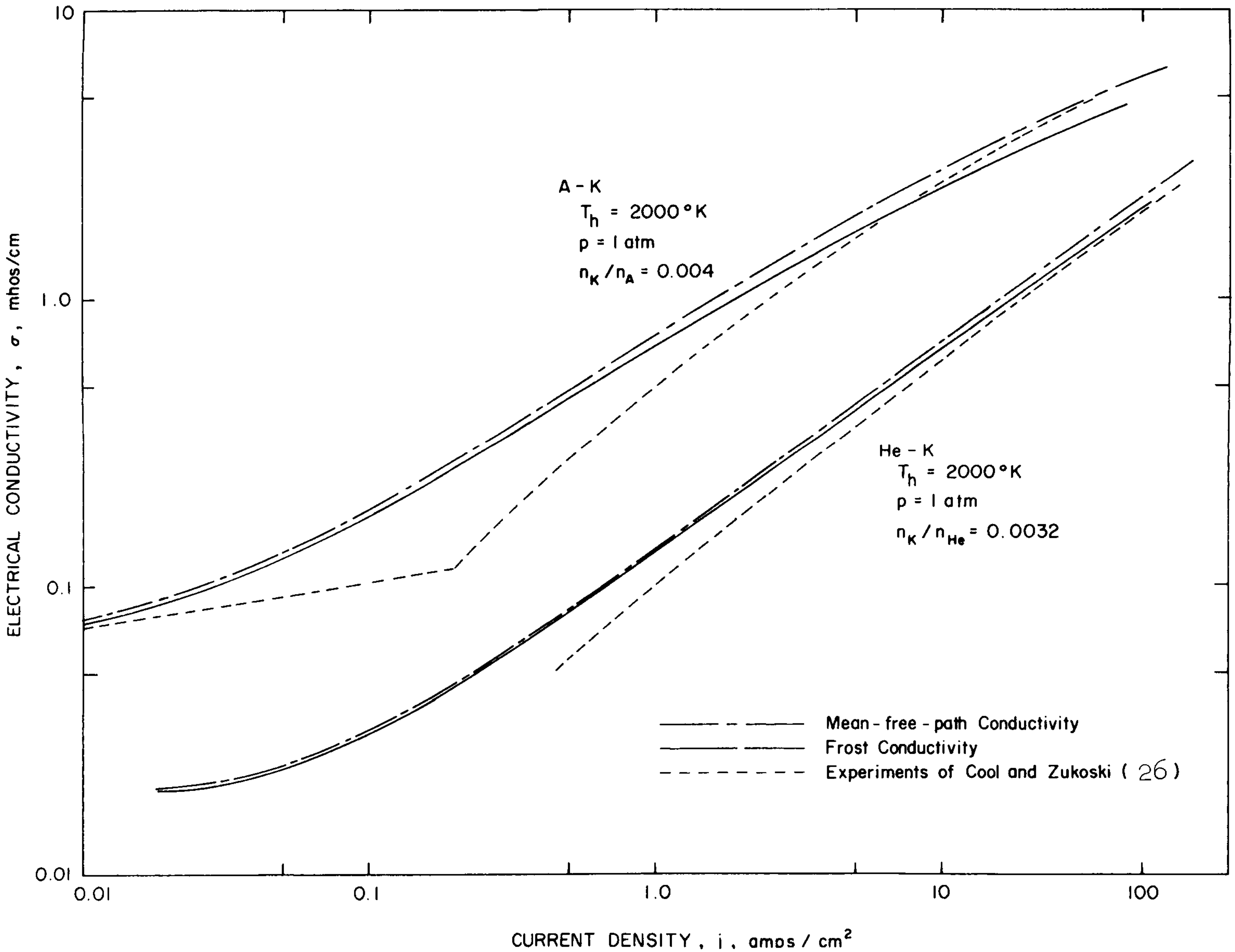

Figure 19. Comparison of calculated electrical conductivities with the data of Cool and Zukoski.

As long as electron-electron collisions are unimportant in the Boltzmann equation, increases in electric field tend to drive the distribution function towards a Lorentz distribution. On the other hand, an increase in electric field increases the electron temperature and consequently the electron number density. Eventually electron-electron collisions become important and drive the distribution toward a Maxwellian at the electron temperature. The actual distribution function resulting from these two effects is very nearly Maxwellian at low electron energies due to the large Coulomb cross section but drops off rapidly at high electron energies as the Coulomb cross section decreases.

The remarkable result from these calculations is that the coupled effects of radiation escape and a non-Maxwellian distribution function can cause much larger deviations from the Saha equation than those that occur when either effect is considered independently.

At present the computer program used in these calculations is being refined so as to include nonelastic-collision terms in the Boltzmann equations.

Publications:
(1) Viegas, J. R. and Kruger, C. H., "Electron Distribution Function in a Nonequipartition Plasma," Seventh Symposium on Engineering Aspects of Magnetohydrodynamics, Princeton University, 1966. (A complete report on this work has been submitted to the Physics of Fluids.)
(2) Viegas, J. R., Ph.D. thesis, Department of Mechanical Engineering, Stanford University.
(3) Shaw, J. F., Kruger, C. H., Mithcner, M. and Viegas, J. R., "Examination of the Validity of the Saha Equation in a Gas Discharge," International Symposium on MHD Electrical Power Generation, Salzburg, 1966.

4.2 The Electrical Conductivity of a Partially Ionized Gas in a Magnetic Field

When a partially ionized gas is subjected to applied electric and magnetic fields $\underline{E}$ and $\underline{B}$ respectively, the resulting current density is [28,29]

$$\underline{J} = \sigma^{\parallel}\underline{E}^{\parallel} + \sigma^{\perp}\underline{E}^{\perp} + \sigma^{H}\,\hat{\underline{B}} \times \underline{E}\ ,$$

where $\underline{B} = B\hat{\underline{B}}$, $\underline{E}^{\parallel} = \underline{E}\cdot\hat{\underline{B}}$, and $\underline{E}^{\perp} = \underline{E} - \underline{E}^{\parallel}$. For small $\underline{E}$, the Chapman-Enskog method provides a means for calculating the tensor conductivity components ($\sigma^{\parallel}$, $\sigma^{\perp}$, σ^{H}) to any desired order of approximation ξ ($\xi = 1, 2, \ldots$). For a partially ionized gas consisting of ν species, this calculation involves the inversion of matrices of order $\nu \times \xi$. Using the fact that the electron mass m_e is much less than the mass of any other particle, it has been shown [30] that the calculation may be simplified so as to require the inversion of matrices of order ξ, independent of the number of species.

Special results are available for two limiting cases. For a very weakly ionized (Lorentzian) gas, there exist particularly simple closed-form expressions [28] which correspond to the $\xi = \infty$ approximation in the Chapman-Enskog sense

$$\sigma^{\perp} = \frac{8}{3\sqrt{\pi}} \frac{n_e e^2}{m_e} \left(\frac{m_e}{2k\ T}\right)^{\frac{5}{2}} \int_0^{\infty} g^4 e^{-m_e g^2/2kT} \frac{\nu_e(g)}{\nu_e(g)^2 + \omega^2} dg \ ,$$

$$\sigma^{H} = \frac{8}{3\sqrt{\pi}} \frac{n_e e^2}{m_e} \left(\frac{m_e}{2k\ T}\right)^{\frac{5}{2}} \int_0^{\infty} g^4 e^{-m_e g^2/2kT} \frac{\omega}{\nu_e(g)^2 + \omega^2} dg \ ,$$

$$\sigma'' = \lim_{\omega \to 0} \sigma^{\perp} \ .$$

The electron number density, charge, and cyclotron frequency are denoted by n_e, $-e$, and $\omega = eB/m_e$ respectively, and B is the magnetic induction. The quantity T denotes the temperature of the gas, k is Boltzmann's constant, and the speed-dependent electron collision frequency is $\nu_e(g) = \sum_n \nu_{en}(g)$, where $\nu_{en}(g)$ is the momentum transfer collision frequency of an electron with the neutral species n. For a fully ionized gas, the Spitzer-Härm [23] value for σ'' corresponds to the $\xi = \infty$ approximation; for $\sigma^{\perp}$ and σ^H, closed-form expressions are available [29,31] for $\xi \leq 3$, and numerical results [32] are available for $\xi \leqq 6$. The numerical results are for $\omega\tau_{ei} \leqq 6$, where

$$\tau_{ei} = \frac{6\sqrt{2}\ \pi^{3/2}\ \epsilon_o^2\ m_e^{1/2}\ (kT)^{3/2}}{n_e\ e^4\ \ell n\Lambda}$$

is a measure of the time between electron-ion collisions.

The results for a Lorentzian gas have been used to examine the speed of convergence of successive Chapman-Enskog approximations. For σ'', the convergence characteristics of a large variety of actual gases were found to be well represented by the mathematical models $\nu_e(g) \propto g^{2m}$, with m in the range $-3/2 \leqq m \leqq 1.5$. These models were then used to examine the convergence characteristics of $\sigma^{\perp}$ and σ^H tend to be slow for $\omega/\overline{\nu_{en}} \lesssim O(1)$, ($\overline{\nu}_{en}$ is a weighted average of $\nu_{en}(g)$), but convergence generally improves as $\omega/\overline{\nu_{en}}$ increases. For a fully-ionized gas, the convergence of σ^H is excellent at $\xi = 2$, but the convergence of $\sigma^{\perp}$ is somewhat slow for

$\omega\tau_{ei} \approx O(6)$, ($\sigma^{\perp}$ is about 15 per cent larger at $\xi = 3$ than at $\xi = 6$).

For the situation of an arbitrary degree of ionization, the Chapman-Enskog calculations are relatively lengthy, and the general practice has been to rely on the approximate mean-free-path results

$$\sigma^{\perp} = \frac{\sigma''}{1 + (\omega/\bar{\nu}_e)^2} \quad , \quad \sigma^H = \left(\frac{\omega}{\bar{\nu}_e}\right)\sigma^{\perp} \, .$$

The method of determining $\bar{\nu}_e$ is not well defined, and again the general practice has been to use a $\bar{\nu}_e$ defined by the parallel conductivity in accordance with the equation $\sigma'' = n_e e^2/m_e \bar{\nu}_e$. We have compared results using these mean-free-path formulas with corresponding calculations based on the simplified Chapman-Enskog method with $\xi = 3$. The comparison varies widely depending on the collision frequency model, the degree of ionization, and on $(\omega/\bar{\nu}_e)$, but in general the mean-free-path formulas yield results which may differ by as much as a factor of 2 with the more accurate calculations.

In order to obtain formulas which are still relatively simple to apply but yield improved accuracy, we have examined extending the method suggested by Frost [33] for calculating σ''. When collisions between charged particles are not negligible, we interpret the $\nu_e(g)$ appearing in the Lorentzian formulas for $\sigma^{\perp}$ and σ^H as

$$\nu_e(g) = \sum_n \nu_{en}(g) + \nu_{ei}(g)$$

where

$$\nu_{ei}(g)^{\perp,H} = \frac{0.476\sqrt{2}}{4\pi\,\epsilon_o^{\,2}} \; \frac{n_e \, e^4 \, \ell n \, \Lambda}{m_2^{3/2}(kT)^{3/2}} \; \frac{h^{\perp,H}(\omega\tau_{ei})}{g^2} \, .$$

The functions $h^{\perp,H}(\omega\tau_{ei})$ are determined by the requirement that when $\sum_n \nu_{en} = 0$, the Lorentzian formulas yield the fully ionized results to the highest order of accuracy available. These functions are shown in Fig. 20 calculated using the 11th Chapman-Enskog approximations for $\sigma^{\perp}$ and σ^H .

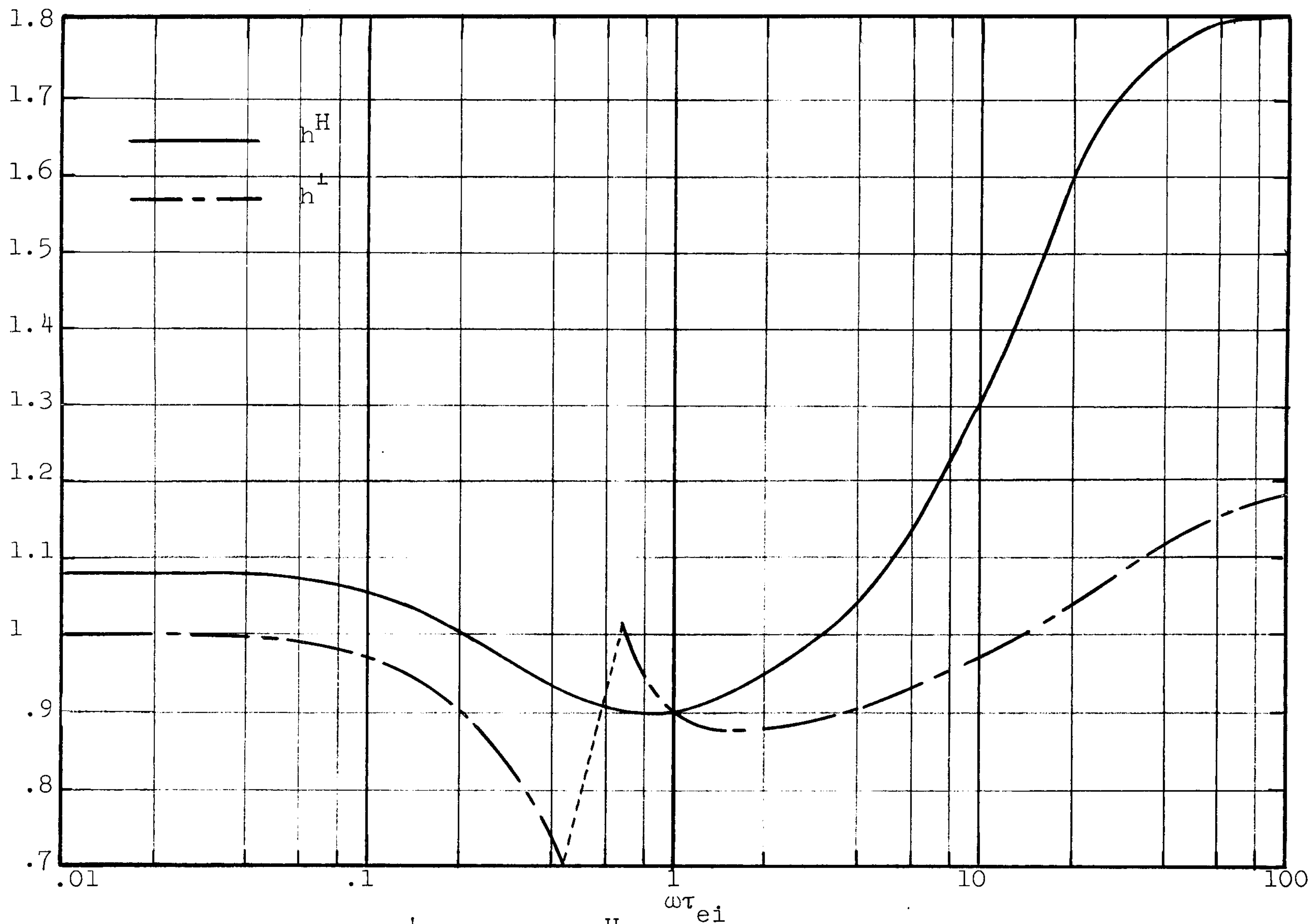

Figure 20. The functions $h^\perp(\omega\tau_{ei})$ and $h^H(\omega\tau_{ei})$ to be used in the proposed mixture rule for calculating the perpendicular and transverse electrical conductivities in a partially ionized gas.

We have compared results using this mixture rule to those obtained by the simplified Chapman-Enskog method with $\xi = 3$. For a large range of collision-frequency models and values of ω, and for all degrees of ionization, we conclude that this proposed mixture yields results which are within a factor of about 15 per cent of the more accurate results.

The work summarized in this section has been reported on in the following references:

(1) Schweitzer, S. and Mitchner, M., "Electrical Conductivity of Partially Ionized Gases," Stanford University Institute for Plasma Research, SUIPR Report No. 56 (Feb. 1966).

(2) Schweitzer, S. and Mitchner, M., "Electrical Conductivity of Partially Ionized Gases," AIAA Journal 4, 1012 (1966).

(3) Schweitzer, S. and Mitchner, M., "The Third Chapman-Enskog Approximation to the Electrical Conductivity of Fully Ionized Gas in a Magnetic Field," Phys. Fluids 8, 2300 (1965).

(4) Schweitzer, S. and Mitchner, M., "The Electrical Conductivity of a Partially Ionized Gas in a Magnetic Field," Seventh Symposium on Engineering Aspects of MHD, Princeton (1965).

(5) Quarterly Reports on Plasma Diagnostics Study for the periods April 1 - June 30 (1965), July 1 - September 30 (1965), January 1 - March 31 (1966).

4.3 Current and Potential Distributions in Finitely Segmented MHD Generators with Nonuniform Electrical Conductivity

In early studies of the nature of electrical conduction in an ionized fluid in segmented electrode MHD generator structures [34-39] attention was directed to the electrodynamic aspect of the problem based on the assumption that the fluid was a medium of uniform electrical conductivity. The currents were then related to the electric field by a simple "Ohm's Law" and the problem could be treated as a classical problem in potential theory.

Recently, however, attempts to understand the results of experiments with segmented electrode MHD generator configurations have stimulated interest in the effects in the conduction process which are peculiarly due to non-uniformities in the fluid [40,41]. Because of the finite size of segmented electrodes and the Hall effect, the current distribution in such structures is non-uniform and hence produces non-uniform Joulean heating. The resulting non-uniform electron temperature leads to a non-uniform electrical conductivity which in turn influences the distribution of current. Other mechanisms are present which may play a role in determining the electron temperature, conductivity, potential, and current distributions, and their importance must still be assessed. Among these are convection, conduction, ionization, radiation loss, diffusion of electrons due to electron pressure and temperature gradients, diffusion of ions, finite rate ionization and recombination, and sheath and emission-absorption effects at the electrode and insulator surfaces.

The two dimensional current flow in the (x,y) plane, the current distribution $\underline{J}(J_x, J_y)$ is governed by the equation

$$\nabla \cdot \underline{J} = 0 \ . \tag{18}$$

With strong applied or induced electric fields, the diffusion of charge may be assumed to result from the gradient of the ϕ (x, y), rather than from temperature and pressure gradients. Assuming also that the ion current is negligible, the generalized Ohm's law leads to the equations

$$J_x = \frac{\sigma(x,y)}{1 + \beta^2} \left[\beta \frac{\partial\Phi}{\partial y} - \frac{\partial\Phi}{\partial x}\right] \ , \tag{19}$$

$$J_y = \frac{\sigma(x,y)}{1 + \beta^2} \left[- \frac{\partial\Phi}{\partial y} - \beta \frac{\partial\Phi}{\partial x}\right] \ , \tag{20}$$

where $\Phi(x,y)$ is defined by

$$\phi = \Phi - \int_0^y u(\xi)\ B\ d\xi \ . \tag{21}$$

The quantity $u(y)$ is the fluid mass velocity assumed to be known and to flow in the x-direction, and B is the applied magnetic induction assumed to be constant and to lie along the z-axis. The quantity β is the Hall parameter. The electrical conductivity $\sigma(x,y)$ is given by the simple mean-free-path result

$$\sigma(x,y) = \frac{n_e(x,y)e^2}{m_e \nu_e} \quad , \tag{22}$$

where $n_e(x,y)$ is the electron number density, $-e$ the electron charge, m_e the electron mass, and ν_e the average momentum transfer electron collision frequency. The conductivity distribution $\sigma(x,y)$ is determined from $n_e(x,y)$ and in an exact calculation, $n_e(x,y)$ is determined by solving the appropriate fluid species conservation equations.

Two cases have been considered for the study of the effects of a non-uniform conductivity. In the first, the electrical conductivity distribution is assumed, and the above equations are then solved for $\Phi(x,y)$ and $J(x,y)$. The implications of particular distributions of conductivity with regard to $\Phi(x,y)$ and $J(x,y)$ may then be examined. In the second case, the electron number density is determined by the electron temperature in the Saha equation assuming that ionization equilibrium prevails. The electron temperature is in turn determined by the electron energy equation. Hence one considers $\sigma = \sigma(n_e)$ and $n_e = n_e\ [T_e(x,y)]$ where, in the absence of convection, conduction, and non-elastic collision effects, the energy equation for $T_e(x,y)$ is

$$\frac{3}{2} k\, n_e(T_e)\nu_e \left(2\frac{m_e}{m_h}\right)(T_e - T) = \frac{J^2(x,y)}{\sigma(T_e)} \quad , \tag{23}$$

where m_h is the average heavy particle mass and k is the Boltzmann constant. Proceeding in this manner, if the heavy particle temperature, T, is assumed known, then equations (18 - 20), (22), and (23) may be solved simultaneously for $\Phi(x, y)$ and $T_e(x,y)$.

The boundary conditions for both these cases on $\Phi(x,y)$ are:

at an electrode
(in the x-z plane)

$$\frac{\partial\Phi}{\partial x} = 0 \text{ or } \Phi = \text{constant}$$

at an insulator
(in the x-z plane)

$$J_Y = 0 \text{ or } \frac{\partial\Phi}{\partial y} = -\beta\,\frac{\partial\Phi}{\partial x} \quad .$$

Some investigators [42] have proposed boundary conditions which may in some sense model electrical phenomena at the gas-surface interface; however, in the interest of explicitly revealing the role of volume effects, we shall neglect interface effects entirely and assume that the conducting surfaces in contact with the gas are infinitely conducting, and the potential of the gas and the conducting surface are identical at the conducting surface. Insulating surfaces in contact with the gas are assumed infinitely non-conducting.

Solutions of the equations for the cases described above have been obtained numerically. The effects of a region of either high or low conductivity near the electrodes relative to the channel center were examined using an assumed conductivity profile in which the conductivity either increased or decreased linearly near the electrode walls. It was found that when the conductivity was high near the electrode wall, the concentration of current near the electrode edge was increased and the difference in voltage between successive electrode pairs (Hall Voltage) was decreased relative to the uniform conductivity case. When the conductivity near the electrode wall was low, the current distribution over the electrode was more uniform but the Hall voltage difference between successive electrodes was negligibly changed relative to the uniform conductivity case.

When the electron number density is determined by the Saha equation at the electron temperature, it is found that the potential equation need not remain of elliptic type. For sufficiently large Hall parameters, the equation becomes hyperbolic. The condition for hyperbolic behavior is precisely equivalent to that for physical instability of the time-dependent electron energy equation. It can be shown that this physical instability corresponds to the condition where the rate of Joulean heating of the electrons exceeds the rate at which the electrons can lose energy by collisions to the heavy particles. For conditions characteristic of an MHD generator, the Φ-equation is uniformly elliptic for $\beta \lesssim 1$. Calculations made under these conditions indicate an increased current concentration at the electrode edge and a decreased Hall voltage between successive electrode pairs. The internal impedance is markedly higher than that for ideal segmented conductors, but still somewhat below that for continuous electrodes with nonequipartition electron heating.

Some typical results for the calculated current distribution are illustrated in Fig. 21. The work summarized in this section has been reported in the following references:

(1) Oliver, D. A. and Mitchner, M., "Nonuniform Electrical Conduction in Magnetophdrodynamic Channels," submitted to AIAA Journal.

(2) Oliver, D. and Mitchner, M., "Current and Potential Distributions in Finitely Segmented MHD Generators with Nonuniform Electrical Conductivity," Seventh Symposium on Engineering Aspects of HMD, Princeton (1965).

(3) Quarterly Reports on Plasma Diagnostics Study for the periods July 1 - September 30 (1965), October 1 - December 31 (1965), January 1 - March 31 (1966), April 1 - June 30 (1966).

5.0 CONCLUSIONS AND RECOMMENDATIONS

The following conclusions may be drawn from the research program described in this report:

1. The interference-filter photographic technique provides a simple method for obtaining spatially resolved electron-temperature measurements in a gas discharge with or without magnetic fields.

2. The electron number density was shown to be greatly out of equilibrium with the electron or gas temperature after expansion in a supersonic nozzle.

3. Conducting deposits on boron-nitride test section walls represent a serious experimental problem.

4. Wall leakage and non-uniformities seriously degrade MHD generator performance.

5. The electron distribution function for a two-temperature gas may be non-Maxwellian for some conditions of electric field and elective density may show large deviations from the Saha equation value.

6. The tensor components of the electrical conductivity of a partially ionized gas in a magnetic field may be found by a mixing rule which compares well with the more complicated Chapman-Enskog method.

7. Non-uniform conductivity profiles in an MHD generator lead to a deterioration of performance. A low conductivity layer adjacent to the electrodes reduces current concentration while a high conductivity layer has the opposite effect.

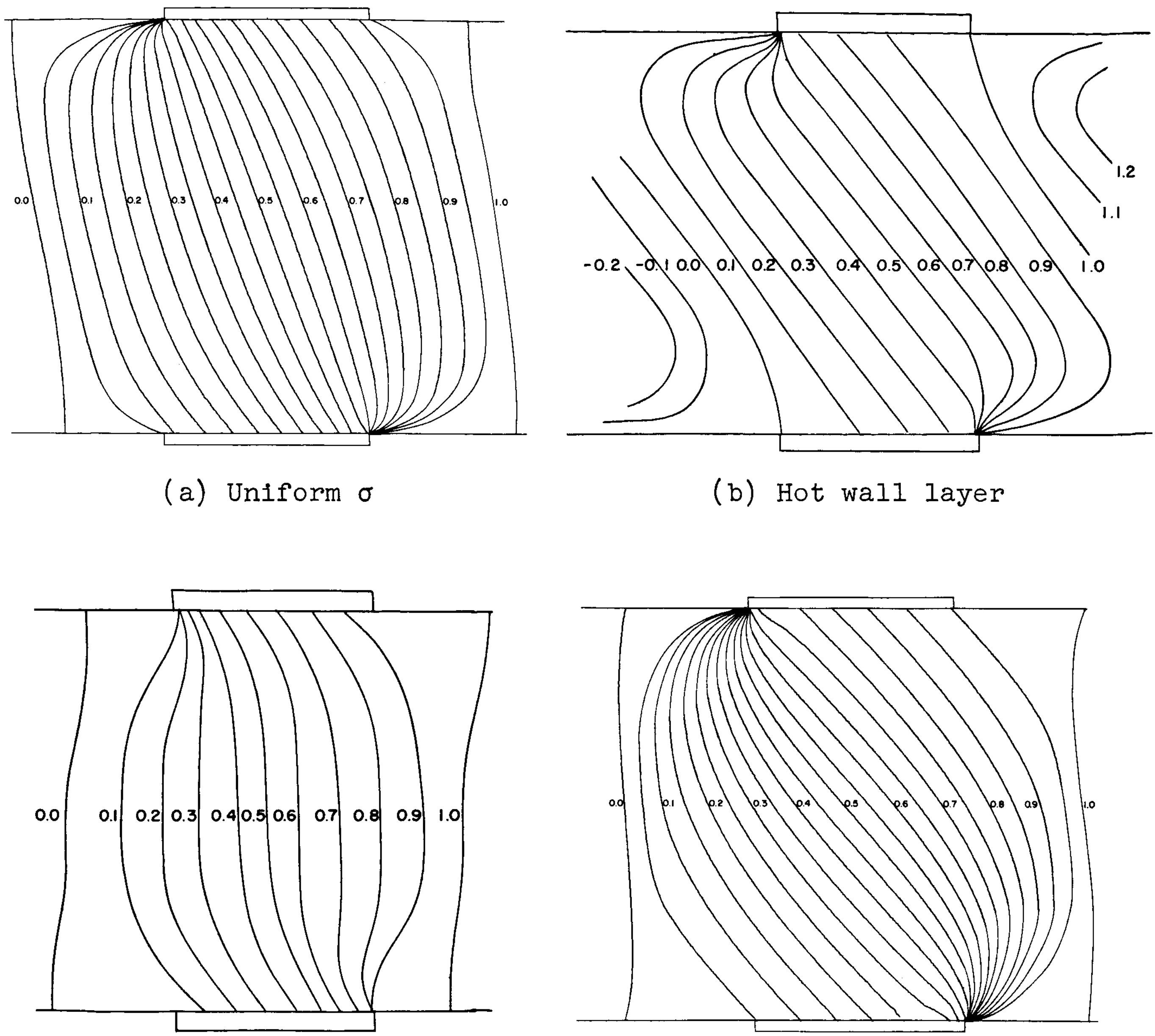

(a) Uniform σ

(b) Hot wall layer

(c) Cold wall layer

(d) Nonequilibrium σ

Figure 21. Effect of nonuniform conductivity on current distribution. All cases are for $\beta = 1$, ratio of period length to channel height of 1, and ratio of electrode length to period length of 1/2. In both cases (b) and (c), the ratio of layer thickness to electrode height is 0.2. In cases (b) and (c) the ratio of wall conductivity to core conductivity is 5 and 0.2 respectively. Case (d) is for a cesium-argon mixture at one atmosphere and a gas temperature of 2400°K; the seed fraction is .004 and the effective electric field is 40 volts/m.

It is recommended that future work be undertaken to

1. investigate MHD generator performance with non-conducting walls such as would be obtainable in the absence of the deposits found in the present program.

2. investigate variable temperature electrodes and insulators to determine experimentally the influences of temperature on current concentrations.

3. determine stability effects in MHD generators.

It is strongly believed that more relatively small-scale laboratory experiments can contribute to understanding the problems of noble gas MHD generators and should be undertaken before large devices are constructed.

REFERENCES

1. Kerrebrock, J. L., Engineering Aspects of Magnetohydrodynamics, ed. Manual and Mather (Columbia University Press, 1962), p. 327.

2. Hurwitz, Sutton, and Tamor, "Electron Heating in MHD Power Generation," ARS Journal (August 1962) 1237-1243.

3. Rosebrock, T. L., et al., "Research on Plasma Properties of Magnetoplasmadynamic Power Generators," Report EDR 4637, Final Technical Report, May 1966, Allison Division, General Motors Corp., Indianapolis, Indiana.

4. Bienert, W. B., "Closed-Cycle Magnetoplasmadynamic Electrical Power Generation with Non-Equilibrium Ionization," Final Technical Report, April 1964, Martin Marietta Corp., Baltimore, Maryland.

5. Lindley, B. C., "Research Programme on Magnetoplasmadynamic Power Generation," Final Technical Summary Report, 1964, International Research and Development Co., Ltd., Newcastle-upon-Tyne 6, England.

6. Shair, F. H., "Investigation of an MGD Power Generation Duct," Final Technical Report NASA CR 54124, General Electric Co., Philadelphia, Pennsylvania.

7. Kerrebrock, J. L., "Segmented Electrode Losses in MHD Generators with Nonequilibrium Ionization," Research Report 178, April 1964, AVCO-Everett Research Laboratory, Everett, Massachusetts.

8. Quarterly Report on Plasma Diagnostics Study for the period October 1 - December 31, 1964, prepared for Lewis-NASA by Plasma Gasdynamics Laboratory, Mechanical Engineering Department, Stanford University.

9. Quarterly Report on Plasma Diagnostics Study for the period January 1 - March 31, 1965, prepared for Lewis-NASA by Plasma Gasdynamics Laboratory, Mechanical Engineering Department, Stanford University.

10. Quarterly Report on Plasma Diagnostics Study for the period April 1 - June 30, 1965, prepared for Lewis-NASA by Plasma Gasdynamics Laboratory, Mechanical Engineering Department, Stanford University.

11. Quarterly Report on Plasma Diagnostics Study for the period July 1 - September 30, 1965, prepared for Lewis-NASA by Plasma Gasdynamics Laboratory, Mechanical Engineering Department, Stanford University.

12. Quarterly Report on Plasma Diagnostics Study for the period October 1 - December 31, 1965, prepared for Lewis-NASA by Plasma Gasdynamics Laboratory, Mechanical Engineering Department, Stanford University.

13. Quarterly Report on Plasma Diagnostics Study for the period January 1 - March 31, 1966, prepared for Lewis-NASA by Plasma Gasdynamics Laboratory, Mechanical Engineering Department, Stanford University.

14. Quarterly Report on Plasma Diagnostics Study for the period April 1 - June 30, 1966, prepared for Lewis-NASA by Plasma Gasdynamics Laboratory, Mechanical Engineering Department, Stanford University.

15. Griem, Hans R., Plasma Spectroscopy (McGraw-Hill Book Company, New York, 1964).

16. Holstein, T., Phys. Rev. 83, 1159 (1951).

17. Bray, K. N. C., "Electron-Ion Recombination in Argon Flowing Through a Supersonic Nozzle," High Temperature Aspects of Hypersonic Flow (Pergamon Press, New York, 1963).

18. Hinnov, E. and Hirschberg, J. G., "Electron-Ion Recombination in Dense Plasmas," Phys. Rev. 125, 795-801 (1962).

19. Heald, M. A., and Wharton, C. B., Plasma Diagnostics with Microwaves, (Wiley, 1965).

20. Jacques, C. P., "The Effects of Ionized Media on Electromagnetic Radiation," Lockheed Missiles and Space Division, LMSD-800637, June 1961.

21. Rosa, R. J. "Hall and Ion Slip Effects in a Nonuniform Gas," Phys. Fluids 5, 1081 (1962).

22. Kerrebrock, J. L., "Magnetohydrodynamic Generators with Nonequilibrium Ionization," AIAA J. 3, 591-601 (1965).

23. Spitzer, L. and Härm, R., "Transport Phenomena in a completely Ionized Gas," Phys. Rev. 89, 977-981 (1953).

24. Schweitzer, S. and Mitchner, M., "Electrical Conductivity of Partially Ionized Gases." Stanford University Institute for Plasma Research Report No. SUIPR-18 (June 30, 1965); also Sixth Symposium on Engineering Aspects of Magnetohydrodynamics.

25. Kerrebrock, J. L. and Hoffman, M. A., "Nonequilibrium Ionization Due to Electron Heating: II. Experiments," AIAA J. 2, 1080-1087 (1964).

26. Cool, T. A. and Zukoski, E. E., "Recombination Rates and Nonequilibrium Electrical Conductivity in a Seeded Plasma," Sixth Symposium on Engineering Aspects of Magnetohydrodynamics, University of Pittsburgh (April 1965).

27. Ben-Daniel, D. J. and Tamor, S., "Nonequilibrium Ionization in Magnetohydrodynamic Generators," General Electric Research Laboratory Report RL2922E (1962).

28. Chapman, S. and Cowling, T. G., The Mathematical Theory of Nonuniform Gases (Cambridge University Press, 1952).

29. Marshall, W., "Kinetic Theory of an Ionized Gas, Parts I, II, and III," T/R 2247, T/R 2352, T/R 2419, Atomic Research Establishment, Harwell, England (1958).

30. Schweitzer, S. and Mitchner, M., "Electrical Conductivity of Partially Ionized Gases," Sixth Symposium on Engineering Aspects of MHD, University of Pittsburgh (April 1965).

31. Schweitzer, S. and Mitchner, M., "The Third Chapman-Enskog Approximation to the Electrical Conductivity of Fully Ionized Gas in a Magnetic Field," Phys. Fluids 8, 2300 (1965).

32. Kaneko, S., Phys. Soc. Japan 15, 1685 (1960).

33. Frost, L. S., "Conductivity of Seeded Atmospheric Pressure Plasmas," J. Appl. Phys. 32, 2029-2039 (1961).

34. Hurwitz, H., Sutton, G. W., and Kilb, H., J. Appl. Phys. 32 205 (1961).

35. Schultz-Grunow, F. and Denzel, D. L., "Evaluation of the Performance Characteristics of a Faraday Generator," Engineering Developments in Energy Conversion (ASME, New York, 1965).

36. Dzung, L. S., "The Magnetohydrodynamic Generator with Hall Effect at the Duct Ends," Brown Boveri Review 49, 6 (1962).

37. Sutton, G. W., "End Losses in Magnetohydrodynamic Channels with Tensor Electrical Conductivity and Segmented Electrodes," J. Appl. Phys. 34, 2 (1963).

38. Fishman, F., "Effect of Electrode Nonuniformities Along the Magnetic Field in MHD Generators," AVCO-Everett Research Report 176 (1963).

39. Crown, J. C., "Analysis of Magnetogasdynamic Generators Having Segmented Electrodes and Anisotropic Conductivity," United Aircraft Corporation Report R-1 852-2(196).

40. Kerrebrock, J. L., AVCO-Everett Research Report 201 (1965).

41. Sherman, F. S., "Nonequilibrium Ionization and Magnetohydrodynamic Phenomenon," General Electric Space Sciences Laboratory Report R64SD36 (1964).

42. Rogers, J. W., "A Theoretical Investigation of the Inlet Current Distribution in an MHD Channel," S. M. Thesis, Massachusetts Institute of Technology, June 1964.

DISTRIBUTION LIST FOR FINAL REPORT

Contract NAS3-6261

National Aeronautics & Space Administration (2)
Washington, D.C. 20546
Attention: RNT/James Lazar

National Aeronautics & Space Administration (1)
Washington, D.C. 20546
Attention: RNT/Jerry Mullin

National Aeronautics & Space Administration (1)
Washington, D.C. 20546
Attention: RRE/Dr. H. Harrison

National Aeronautics & Space Administration (2)
Washington, D.C. 20546
Attention: RNP/Dr. F. Schulman

National Aeronautics & Space Administration (1)
Washington, D.C. 20546
Attention: RNP/James Lynch

National Aeronautics & Space Administration (1)
Washington, D.C. 20546
Attention: RRP/Dr. K. H. Thom

NASA Lewis Research Center (1)
21000 Brookpark Road
Cleveland, Ohio 44135
Attention: Spacecraft Technology Procurement Section (M.S. 54-2)

NASA Lewis Research Center (1)
21000 Brookpark Road
Cleveland, Ohio 44135
Attention: C. C. Conger

NASA Lewis Research Center (1)
21000 Brookpark Road
Cleveland, Ohio 44135
Attention: D. L. Lockwood

NASA Lewis Research Center (3)
21000 Brookpark Road
Cleveland, Ohio 44135
Attention: N. J. Stevens

NASA Lewis Research Center (1)
21000 Brookpark Road
Cleveland, Ohio 44135
Attention: Bernard Lubarsky

NASA Lewis Research Center (1)
21000 Brookpark Road
Cleveland, Ohio 44135
Attention: Robert English

NASA Lewis Research Center (1)
21000 Brookpark Road
Cleveland, Ohio 44135
Attention: L. Nichols

NASA Lewis Research Center (1)
21000 Brookpark Road
Cleveland, Ohio 44135
Attention: Henry Slone

NASA Lewis Research Center (1)
21000 Brookpark Road
Cleveland, Ohio 44135
Attention: Reports Control Office (M.S. 5-5)

NASA Lewis Research Center (1)
21000 Brookpark Road
Cleveland, Ohio 44135
Attention: Technology Utilization Officer (M.S. 3-19)

NASA Lewis Research Center (4)
21000 Brookpark Road
Cleveland, Ohio 44135
Attention: Library (M.S. 60-3)

Aeronautical Systems Division (1)
Flight Accessories Laboratories
Wright Field AFB, Ohio
Attention: Robert Barthelemy APIE-2

Aeronautical Systems Division (1)
Flight Accessories Laboratories
Wright Field AFB, Ohio
Attention: Eric Soengen

Office of Naval Research (1)
Washington, D. C. 20025
Attention: Dr. Ralph Roberts

DISTRIBUTION LIST FOR FINAL REPORT

Contract NAS3-6261

National Aeronautics & Space Administration (2)
Washington, D.C. 20546
Attention: RNT/James Lazar

National Aeronautics & Space Administration (1)
Washington, D.C. 20546
Attention: RNT/Jerry Mullin

National Aeronautics & Space Administration (1)
Washington, D.C. 20546
Attention: RRE/Dr. H. Harrison

National Aeronautics & Space Administration (2)
Washington, D.C. 20546
Attention: RNP/Dr. F. Schulman

National Aeronautics & Space Administration (1)
Washington, D.C. 20546
Attention: RNP/James Lynch

National Aeronautics & Space Administration (1)
Washington, D.C. 20546
Attention: RRP/Dr. K. H. Thom

NASA Lewis Research Center (1)
21000 Brookpark Road
Cleveland, Ohio 44135
Attention: Spacecraft Technology Procurement Section
(M.S. 54-2)

NASA Lewis Research Center (1)
21000 Brookpark Road
Cleveland, Ohio 44135
Attention: C. C. Conger

NASA Lewis Research Center (1)
21000 Brookpark Road
Cleveland, Ohio 44135
Attention: D. L. Lockwood

NASA Lewis Research Center (3)
21000 Brookpark Road
Cleveland, Ohio 44135
Attention: N. J. Stevens

NASA Lewis Research Center (1)
21000 Brookpark Road
Cleveland, Ohio 44135
Attention: Bernard Lubarsky

NASA Lewis Research Center (1)
21000 Brookpark Road
Cleveland, Ohio 44135
Attention: Robert English

NASA Lewis Research Center (1)
21000 Brookpark Road
Cleveland, Ohio 44135
Attention: L. Nichols

NASA Lewis Research Center (1)
21000 Brookpark Road
Cleveland, Ohio 44135
Attention: Henry Slone

NASA Lewis Research Center (1)
21000 Brookpark Road
Cleveland, Ohio 44135
Attention: Reports Control Office (M.S. 5-5)

NASA Lewis Research Center (1)
21000 Brookpark Road
Cleveland, Ohio 44135
Attention: Technology Utilization Officer (M.S. 3-19)

NASA Lewis Research Center (4)
21000 Brookpark Road
Cleveland, Ohio 44135
Attention: Library (M.S. 60-3)

Aeronautical Systems Division (1)
Flight Accessories Laboratories
Wright Field AFB, Ohio
Attention: Robert Barthelemy APIE-2

Aeronautical Systems Division (1)
Flight Accessories Laboratories
Wright Field AFB, Ohio
Attention: Eric Soengen

Office of Naval Research (1)
Washington, D. C. 20025
Attention: Dr. Ralph Roberts

Office of Naval Research (1)
Washington, D.C. 20025
Attention: John Satkowski/Room 2509

U. S. AF Office of Scientific Research (1)
Washington, D. C. 20025
Attention: Dr. M. Slawsky

AVCO Everett Research Laboratory (1)
2385 Revere Beach Parkway
Everett, Massachusetts 02149
Attention: T. Brogan

Electrical Engineering Department, MIT (1)
Cambridge, Massachusetts 02139
Attention: Dr. J. Kerrebrock

Electrical Engineering Department, MIT (1)
Cambridge, Massachusetts 02139
Attention: Professor H. H. Woodson

MHD Research, Inc. (1)
1535 Monrovia Street
Newport Beach, California 92660
Attention: Dr. V. H. Blackman

Westinghouse Research & Development Center (1)
Beulah Rd., Churchill Borough
Pittsburgh, Pennsylvania 15235
Attention: Dr. W. Emmerich

General Atomic Division (1)
General Dynamics Corporation
P. O. Box 608
San Diego, California 92115
Attention: Dr. J. Colwell

Martin-Marietta Corporation (1)
Baltimore, Maryland 21203
Attention: Dr. Bienert

General Electric Company (1)
Valley Forge Space Technology Center
Space Sciences Laboratory
P. O. Box 8555
Philadelphia, Pennsylvania 19101
Attention: Dr. A. Sherman

California Institute of Technology (1)
4800 Oak Grove Drive
Pasadena, California 91103
Attention: Dr. F. H. Shair

Chief, Bureau of Ships (1)
Navy Department
Washington, D. C. 20360
Attention: Dr. John Huth, Chief Scientist

Aeronautical Research Associates of
Princeton (1)
Princeton, New Jersey

Atomics International (1)
8900 DeSota Avenue
Canoga Park, California 91304
Attention: Dr. Robert Allen

Institute for Aerospace Studies (1)
University of Toronto
Toronto 5, Canada
Attention: Dr. S. Townsend

NASA Scientific & Technical Information
Facility (6)
P. O. Box 33
College Park, Maryland 20740
Attention: NASA Representative RQT-2448

AFWL (1)
Kirtland AFB, New Mexico
Attention: Capt. C. F. Ellis/WLPC

Aerospace Corporation (1)
P. O. Box 95085
Los Angeles, California 90045
Attention: Library Technical Documents Group

Westinghouse Astronuclear Laboratories (1)
Electric Propulsion Laboratory
Pittsburgh, Pennsylvania 15234
Attention: Mr. H. W. Szymanowski